AMERICAN SOCIETY FOR MICROBIOLOGY | mBio

Check for updates

| Editor's Pick | Parasitology | Research Article

Additional PfCRT mutations driven by selective pressure for improved fitness can result in the loss of piperaquine resistance and altered *Plasmodium falciparum* physiology

Laura M. Hagenah,[1,2] Satish K. Dhingra,[1,2] Jennifer L. Small-Saunders,[2,3] Tarrick Qahash,[4,5] Andreas Willems,[6,7] Kyra A. Schindler,[1,2] Gabriel W. Rangel,[5] Eva Gil-Iturbe,[8] Jonathan Kim,[9] Emiliya Akhundova,[9] Tomas Yeo,[1,2] John Okombo,[1,2] Filippo Mancia,[9] Matthias Quick,[8,9,10] Paul D. Roepe,[6,7] Manuel Llinás,[4,5] David A. Fidock[1,2,3]

AUTHOR AFFILIATIONS See affiliation list on p. 17.

ABSTRACT Malaria elimination efforts in Southeast Asia have been hindered by multidrug-resistant *Plasmodium falciparum*. High-grade resistance to piperaquine (PPQ, used in combination with dihydroartemisinin) is associated with PfCRT mutations that arose in strains expressing the PfCRT Dd2 isoform, which mediates resistance to the related 4-aminoquinoline chloroquine (CQ). The PPQ-resistant PfCRT haplotype Dd2 + F145I mediates the highest level resistance but causes a significant growth defect in intra-erythrocytic parasites. Recently, three separate mutations (F131C, I347T and C258W) have been observed on Dd2 + F145I PfCRT either during extended parasite culture or in Southeast Asian isolates no longer subject to PPQ pressure. Competitive growth assays with *pfcrt*-edited parasites reveal that these compensatory mutations reduce the fitness defect caused by F145I. PPQ survival assays on edited lines show a loss of PPQ resistance in two of the three variants, including the field mutant (C258W). The latter restores CQ resistance. None of these variants alter parasite susceptibility to the first-line partner drug, mefloquine. Utilizing drug transport assays with purified PfCRT isoforms reconstituted into proteoliposomes, we identify differences in mutant PfCRT-mediated transport of PPQ and CQ. Molecular dynamics energy minimization calculations predict that these same mutations cause small but significant conformational changes in PfCRT regions implicated in drug interactions. Metabolomic analyses of isogenic parasite lines reveal differences in hemoglobin-derived peptide accumulation as a hallmark of PfCRT variation. These studies highlight the transient nature of PPQ resistance upon removal of drug pressure and suggest a strategy for employing this drug as part of multiple first-line therapies.

IMPORTANCE Our study leverages gene editing techniques in *Plasmodium falciparum* asexual blood stage parasites to profile novel mutations in mutant PfCRT, an important mediator of piperaquine resistance, which developed in Southeast Asian field isolates or in parasites cultured for long periods of time. We provide evidence that increased parasite fitness of these lines is the primary driver for the emergence of these PfCRT variants. These mutations differentially impact parasite susceptibility to piperaquine and chloroquine, highlighting the multifaceted effects of single point mutations in this transporter. Molecular features of drug resistance and parasite physiology were examined in depth using proteoliposome-based drug uptake studies and peptidomics, respectively. Energy minimization calculations, showing how these novel mutations might impact the PfCRT structure, suggested a small but significant effect on drug interactions. This study reveals the subtle interplay between antimalarial resistance, parasite fitness, PfCRT structure, and intracellular peptide availability in PfCRT-mediated parasite responses to changing drug selective pressures.

Editor Thomas E. Wellems, National Institute of Allergy and Infectious Diseases, Bethesda, Maryland, USA

Address correspondence to David A. Fidock, df2260@cumc.columbia.edu.

The authors declare no conflict of interest.

See the funding table on p. 17.

Received 12 July 2023
Accepted 31 October 2023
Published 7 December 2023

KEYWORDS *Plasmodium falciparum*, malaria, drug resistance evolution, fitness, *PfCRT*

Morbidity and mortality rates of *Plasmodium falciparum* malaria continue to be exceedingly high, with an estimated 241 million cases and 619,000 deaths in 2021 (1). Artemisinin (ART)-combination therapies (ACTs) serve as the first-line treatment for *P. falciparum* worldwide (2). This treatment consists of a potent yet rapidly eliminated ART derivative that is paired with a longer lasting partner drug, such as mefloquine (MFQ), amodiaquine, or piperaquine (PPQ), to eliminate residual parasites. Unfortunately, a major threat to the efficacy of these treatments is the recent emergence and spread of *P. falciparum* strains that are resistant to one or both ACT components (3).

PPQ has numerous benefits as an ACT partner drug, including its safety profile in children and pregnant women, its potency against chloroquine (CQ)-resistant parasites, and its long half-life (~20–30 days). The pharmacokinetics of PPQ enable post-treatment prophylactic effects, which makes the dihydroartemisinin (DHA)-PPQ combination attractive for chemoprevention treatment in regions of Africa (4). DHA-PPQ has proven to be effective for both seasonal malaria chemoprevention (intermittent administration of full treatment courses to children during the malaria season in areas of increased seasonal transmission) and intermittent preventative treatment (administration of full courses to pregnant women and infants to prevent malaria infection in these high-risk groups) (5). In addition, MFQ paired with DHA-PPQ has been proposed as an effective triple combination therapy to impede the development of multidrug-resistant strains (6). For the DHA-PPQ combination, reports of widespread treatment failure in Southeast (SE) Asia raise concerns about its long-term effectiveness and highlight the need to understand mechanisms of PPQ resistance (7).

PPQ, like the related 4-aminoquinoline drug CQ, is believed to accumulate within the parasite's digestive vacuole (DV) where it presumably acts upon the hemoglobin (Hb) degradation pathway. Experimental evidence suggests that PPQ binds to toxic free heme monomers released during Hb proteolysis, thereby preventing their incorporation into chemically inert hemozoin crystals (8). Studies have associated PPQ resistance with mutations in the DV membrane-resident protein PfCRT (*P. falciparum* chloroquine resistance transporter), as confirmed by gene editing (9–16). Evidence suggests that these mutations enable the transporter to efflux positively charged PPQ out of its site of action in the DV (17–19), resulting in parasite survival under high drug concentrations. PPQ-resistant (PPQ-R) PfCRT mutations have also been linked to alterations in Hb metabolism, DV swelling, and decreased parasite fitness (12, 15, 16, 20, 21).

In SE Asia, PPQ-R point mutations arose primarily on parasites expressing the CQ-resistant Dd2 PfCRT, which differs from the 3D7 wild-type (WT) isoform by eight mutations (Table 1) (22). Interestingly, PPQ-R mutations often re-sensitize parasites to CQ, despite the presence of the K76T amino acid substitution that is often used to define CQ resistance-associated PfCRT isoforms. PPQ resistance has also been associated with amplification of *plasmepsins II/III* that encode hemoglobinases (23). Nevertheless, mutant PfCRT haplotypes have been shown to mediate high-level PPQ resistance even in parasites with single copies of these plasmepsins (12). PPQ resistance *in vitro* is characterized by atypical bimodal dose-response profiles and >10% of ring-stage parasites surviving a 48-h exposure to 200 nM PPQ, as measured in the PPQ survival assay (PSA) (9). Resistant parasites *in vitro* also exhibit incomplete parasite killing at elevated PPQ concentrations, manifesting in an increased IC_{90} (the drug concentration that inhibits parasite growth by 90%) (12). Of the SE Asian PPQ-R haplotypes, Dd2 + F145I exhibits the highest levels of survival under PPQ treatment (>25% survival at concentrations of 200 nM PPQ) (12).

In addition to antimalarial susceptibility, parasite fitness influences which strains dominate in the field. In *P. falciparum*, fitness broadly includes the capacity for sexual development and transmission as well as the asexual blood stage (ABS) growth rate. Previous analyses of isogenic parasites expressing variant *pfcrt* alleles have shed light on their ability to influence ABS growth rates and have uncovered important differences

TABLE 1 PfCRT isoforms of edited parasites used in this study[a]

PfCRT isoform	Origin	PfCRT amino acid at listed positions											
		74	75	76	131	145	220	258	271	326	347	356	371
Dd2	SE Asia	I	E	T	F	F	S	C	E	S	I	T	I
Dd2 + F145I	Cambodia	I	E	T	F	I	S	C	E	S	I	T	I
Dd2 + F145I + F131C	Lab	I	E	T	C	I	S	C	E	S	I	T	I
Dd2 + F145I + I347T	Lab	I	E	T	F	I	S	C	E	S	T	T	I
Dd2 + F145I + C258W	SE Asia	I	E	T	F	I	S	W	E	S	I	T	I
3D7 (WT)	E Africa	M	N	K	F	F	A	C	Q	N	I	I	R

[a]*pfcrt* was edited in Dd2 parasites using customized zinc finger nucleases to express the PfCRT isoforms listed above (see Fig. S1). The origin of the PfCRT isoform is noted. E, East; SE, Southeast.

regarding their global spread (24, 25). Among the PPQ-R mutants, the highly resistant Dd2 + F145I allele imparts the most considerable growth defect (12). In contrast, other variants, such as Dd2 + T93S and Dd2 + I218F, have increased rapidly in Cambodia, which can be explained by their combination of relatively high-grade resistance and low fitness cost (15).

In 2016, policy guidelines in Cambodia changed first-line treatment from DHA-PPQ to artesunate-MFQ in response to widespread PPQ resistance (26). However, since large amounts of drug were still circulating in this area, PPQ usage was not officially stopped until years later. Due to the large fitness cost that PPQ-R PfCRT mutations impart on the parasite, we hypothesized that the proportion of parasites with these mutations may decrease in the absence of PPQ pressure. A large genome sequencing effort applied to 20,000 parasite isolates across Asia and Africa (MalariaGEN Pf7) identified additional mutations on Dd2 + F145I PfCRT in SE Asia (27). We also observed this phenomenon with *in vitro* Dd2 + F145I parasites cultured for extended periods of time.

Herein, we utilized gene editing to investigate the impact of recently identified secondary PfCRT amino acid substitutions on parasite fitness and PPQ susceptibility. These studies are of particular importance in determining how the parasite landscape can change following the removal of PPQ pressure. Our data reveal that these novel mutations improve the ABS replication rate of Dd2 + F145I parasites, suggesting evolutionary pressure to diminish the fitness cost imposed by this PfCRT mutation in the absence of PPQ usage. These novel haplotypes confer varying susceptibility to PPQ. To probe deeper into the impact of these mutant PfCRT haplotypes and to further inspect any connection between PfCRT structure and function, we present data on drug transport kinetics and peptidomics for purified PfCRT and genetically edited *P. falciparum* strains, respectively. Collectively, our studies reveal a broad effect of PfCRT mutations on parasite physiology, which underscores the instability of these mutations in SE Asia.

RESULTS

Additional mutations developed on Dd2 + F145I PfCRT

Following an extended period of continuous ABS culture (>60 days) of our gene-edited $Dd2^{Dd2+F145I}$ line (12), we observed an increased growth rate. By sequencing the *pfcrt* locus, we identified two new mutations, F131C and I347T, which appeared independently in this culture. Clones of each mutant line ($Dd2^{Dd2+F145I+F131C}$ and $Dd2^{Dd2+F145I+I347T}$) were obtained using limiting dilution, and whole-genome sequencing confirmed that single-nucleotide polymorphisms in *pfcrt* were the only major difference between these lines and parental $Dd2^{Dd2+F145I}$. Of note, there was no amplification of the *plasmepsins II/III* locus.

We also focused on the Dd2 + F145I + C258W variant that was reported by MalariaGEN investigators as the most prevalent contemporary PfCRT mutation that had recently emerged in eastern SE Asia in isolates carrying PPQ-R PfCRT mutations. This additional mutation was identified in 16 isolates that all harbored the PfCRT Dd2 + F145I mutations (27).

Using customized gene editing (28), we introduced these mutant alleles into a Dd2 parasite in place of its endogenous *pfcrt* allele (Table 1; Fig. S1). Isogenic parasite lines (referred to as edited or "ed") were engineered to express the PfCRT isoforms Dd2 + F145I + F131C, Dd2 + F145I + I347T, or Dd2 + F145I + C258W. For the former two, gene editing was used to independently confirm the impact of the F131C or I347T mutations in the *in vitro*-derived lines. All three lines were compared to $Dd2^{Dd2+F145I}$, their isogenic parent. Our control lines were $Dd2^{Dd2}$ and $Dd2^{3D7}$, which express the CQ-resistant isoform Dd2 and the WT drug-sensitive PfCRT isoform 3D7, respectively (12, 28, 29). Both the edited lines and the original clones were assayed for any changes in parasite fitness or drug susceptibility.

Second-site mutations alleviate the fitness cost imparted by the *pfcrt* Dd2 + F145I allele

To assess the impact of these mutations on ABS parasite growth rates, we used an established flow cytometry-based co-culture assay (12, 15, 24). Parasite cultures were seeded at an approximately 1:1 ratio of a GFP-expressing Dd2 line (Dd2-GFP) and each Dd2 test line (that was GFP negative). Samples were then examined by flow cytometry every 2 to 3 days for 21 days (~10.5 parasite generations) to determine the percentages of GFP^+ parasites. $Dd2^{3D7}$ and $Dd2^{Dd2}$ were the most fit, outcompeting the Dd2-GFP line within a week, with expression of the 3D7 (WT) isoform resulting in the fastest growth rate. Of the new PfCRT variants, only $Dd2^{Dd2+F145I+I347T}$ showed improved fitness relative to the GFP reporter line (Fig. 1A).

From these data, we extrapolated the change in parasite fitness relative to $Dd2^{Dd2}$ by calculating the percent change in growth rate per 48-h generation for each test line (Fig. 1B). The $Dd2^{Dd2+F145I}$ line was the most unfit, with a 23.1% fitness cost per generation, consistent with prior reports (12, 15, 16). When compared to $Dd2^{Dd2+F145I}$, we observed a modest improvement in fitness in $Dd2^{Dd2+F145I+F131C}$ parasites (calculated at 21.5% and 21.2% cost for the original and edited clone, respectively, relative to $Dd2^{Dd2}$). However, the addition of I347T to Dd2 + F145I PfCRT significantly improved the fitness of both the original mutant parasite and the edited clone (10.8% and 11.7% cost, respectively, relative to $Dd2^{Dd2}$). The Dd2 + F145I + C258W isoform, seen in SE Asian parasites, had a diminished fitness cost of only 18.9% relative to $Dd2^{Dd2}$ (compared to the 23.1% cost of the F145I mutation alone). This suggests that the C258W mutation emerged on a Dd2 +F145I PfCRT background to increase parasite ABS growth rate in the absence of sustained PPQ pressure.

Parasites expressing Dd2 + F145I + F131C, Dd2 + F145I + I347T, or Dd2 + F145I + C258W PfCRT displayed distended DVs in the trophozoite stage, similar to other PPQ-R lines, but the vacuoles in the schizont stage appeared to be smaller compared to those in $Dd2^{Dd2+F145I}$ (Fig. S2). This bloating in the trophozoite and schizont stages is a characteristic feature of PPQ-R lines (10, 12, 29).

Novel mutant PfCRT alleles increase parasite sensitivity to PPQ albeit to varying degrees

Using the PSA across a range of concentrations (1,600 nM to 3.1 nM PPQ) (12, 15, 30), we tested our edited and original mutant parasite lines for any changes in PPQ susceptibility. The control line $Dd2^{Dd2+F145I}$ showed high levels of survival across a range of high concentrations (32.9%, 18.4%, and 15.4% survival at 800 nM, 200 nM, and 100 nM PPQ, respectively; Fig. 2A; Table S1). The addition of the F131C mutation to Dd2 + F145I PfCRT did not significantly alter PPQ survival rates for either the original mutant (28.5%, 14.2%, and 14.2% at 800 nM, 200 nM, and 100 nM PPQ, respectively) or the edited line (30.5%, 12.1%, and 10.1% at 800 nM, 200 nM, and 100 nM PPQ, respectively; P value ≥0.05 using Mann-Whitney U tests for both the original and the edited lines as compared to the isogenic $Dd2^{Dd2+F145I}$ line). However, both the I347T and C258W second-site mutations affected PPQ susceptibility. I347T sensitized both the original and the edited clones, which displayed survival rates well below the 10% resistance threshold at 200 nM PPQ

(1.7% and 3.2%, respectively). Similarly, C258W parasites became largely re-sensitized, with 4.3% survival at 200 nM PPQ.

We also measured PPQ susceptibility using 72-h dose-response assays with asynchronous parasite cultures. While all tested lines had similar IC_{50} values (Fig. S3A), only $Dd2^{Dd2+F145I+F131C}$ parasites had sustained growth at high concentrations of PPQ. These clones (original and edited) had comparable mean IC_{90} values to $Dd2^{Dd2+F145I}$ (3.6 µM and 2.8 µM compared to 5.6 µM; Fig. 2B; Table S2). These F131C lines displayed an ~3,000 to 5,000-fold increase compared to the Dd2 mean IC_{90} (24 nM). This is consistent with previous observations that PPQ resistance is only apparent at high drug concentrations, underscoring the importance of the PSA to quantify PPQ resistance instead of relying on IC_{50} metrics.

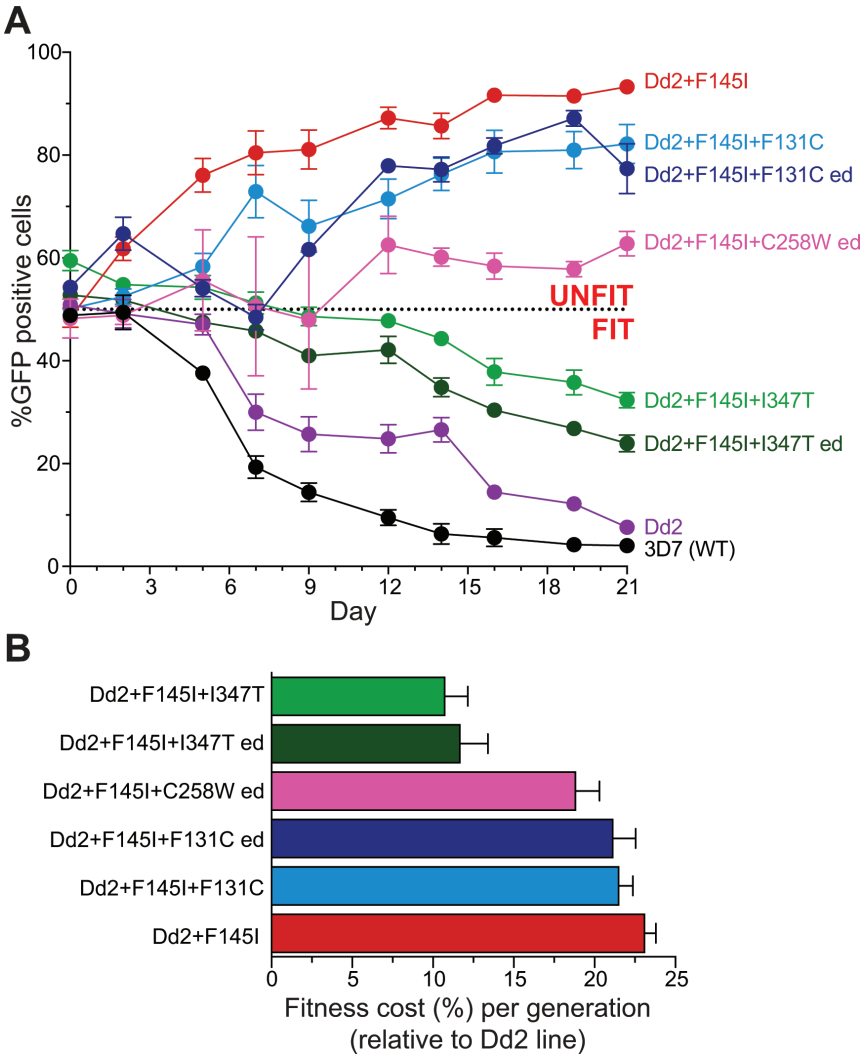

FIG 1 Mutations reduce fitness cost of Dd2 + F145I PfCRT *in vitro*. (A) Isogenic *pfcrt*-modified parasite lines, each generated in the Dd2 strain, were co-cultured at an approximately 1:1 ratio with a reference Dd2 line expressing GFP (Dd2-GFP). The labeling indicates the PfCRT isoform expressed by each gene-edited line. The *pfcrt*-edited (ed) lines expressing Dd2 + F145I + F131C, Dd2 + F145I + C258W, or Dd2 + F145I + I347T were generated using customized zinc finger nucleases. Cultures were analyzed by flow cytometry every 2–3 days up to day 21 (10.5 parasite generations), and the mean ± SEM percentages of GFP^+ parasites were plotted over time. Values above the 50% dashed line indicate that the test line was less fit than Dd2-GFP. (B) Mean ± SEM relative fitness cost shown as a percent reduction in parasite growth per 48-h generation is shown, relative to the isogenic $Dd2^{Dd2}$ line. $N = 2–3$; $n = 2$.

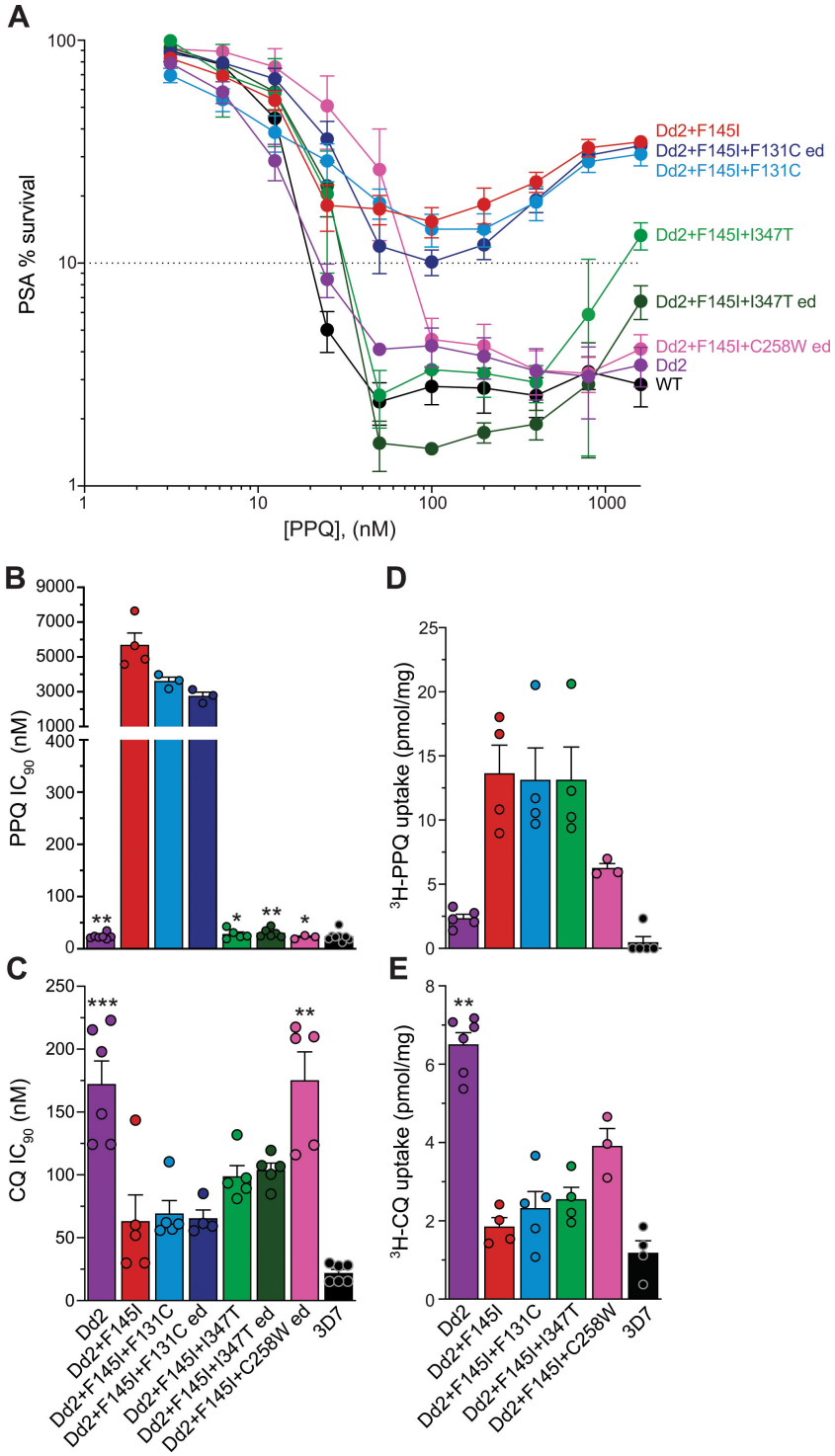

FIG 2 $Dd2^{Dd2+F145I+C258W}$ and $Dd2^{Dd2+F145I+I347T}$ display increased susceptibility to PPQ and altered susceptibility to CQ due to altered drug transport via PfCRT. (A) Survival rates of isogenic *pfcrt*-modified lines, each generated in the Dd2 strain, were determined using the *in vitro* PSA (starting with 0- to 6-h rings and treated for 72 h). The 10% cutoff represents a standard 200 nM threshold for PPQ resistance in this assay (30). The labeling indicates the PfCRT isoform expressed by each recombinant line. "ed" refers to lines where the novel PfCRT mutation (F131C, I347T, or C258W) was gene edited into the $Dd2^{Dd2+F145I}$ parasite line. Survival values are shown in Table S1 as means ± SEM. $N = 7$; $n = 2$. (B and C) Mean ± SEM IC_{90} values (Table S2) were calculated from 72-h concentration-response assays for (B) PPQ and (C) CQ. *N*

(Continued on next page)

FIG 2 (Continued)

= 4–7; *n* = 2. Significance was determined using Mann-Whitney *U* tests. Comparisons are shown between *pfcrt*-edited lines and their isogenic controls. (D and E) Mean ± SEM uptake of 100 nM (D) ^{3}H-PPQ or (E) ^{3}H-CQ was measured for 1 min in proteoliposomes containing the indicated PfCRT variants or in control liposomes. Data are means of *n* = 4–6. *P < 0.05; **P < 0.01; ***P < 0.001. (B–E) Individual circles indicate values from each independent experiment.

Second-site mutations result in altered susceptibility to CQ and monodesethyl-CQ

We next assessed the response of these lines to a set of reference antimalarial drugs. Prior studies revealed that the F145I mutation hypersensitizes parasites to CQ and the primary CQ metabolite monodesethyl (md)-CQ, despite arising on the CQ-resistant Dd2 isoform (12). Our data show that the lab-selected Dd2$^{Dd2+F145I+F131C}$ and Dd2$^{Dd2+F145I+I347T}$ lines retained a CQ-susceptible status (Fig. 2C; Table S2). Interestingly, parasites expressing the field isoform Dd2 + F145I + C258W exhibited increased CQ and md-CQ mean IC_{90} values (175 nM and 1.6 µM, respectively) compared to Dd2$^{Dd2+F145I}$ (63 and 317 nM, respectively). The response of Dd2$^{Dd2+F145I+C258W}$ to these drugs did not statistically differ from that of Dd2^{Dd2} (whose CQ and md-CQ mean IC_{90} values were 172 nM and 1.2 µM, respectively; Fig. 2C; Table S2). There was no change in susceptibility to quinine, md-amodiaquine, or MFQ with any of the original or edited lines (Fig. S3C, D, and F). The pyronaridine (PND) mean IC_{50} value of Dd2$^{Dd2+F145I+C258W}$ showed a small (twofold) albeit significant decrease compared to Dd2$^{Dd2+F145I}$ (P = 0.029 in Mann-Whitney *U* test; Fig. S3E), suggesting that PfCRT mutations can modulate parasite susceptibility to PND.

PfCRT-mediated PPQ and CQ uptake correlates with *in vitro* parasite susceptibility

We next sought to probe the impact of these novel mutations on PPQ and CQ transport via PfCRT. Dd2 + F145I + F131C, Dd2 + F145I + I347T, and Dd2 + F145I + C258W isoforms were heterologously expressed in eukaryotic HEK293 cells and purified, along with Dd2 + F145I (PPQ-R, CQ sensitive), Dd2 (PPQ sensitive and CQ resistant), and 3D7 (PPQ and CQ sensitive) as controls (17). As a proxy for transport, we measured uptake of ^{3}H-PPQ or ^{3}H-CQ by PfCRT-containing proteoliposomes (Fig. 2D and E; Table S3). In this system, an inwardly directed pH gradient (interior alkaline) and electrical transmembrane potential (negative inside) serve as driving forces for PfCRT-mediated drug transport, mimicking the physiological environment under which drug is effluxed out of the parasite DV. Transport studies were performed by adding 100 nM ^{3}H-PPQ or ^{3}H-CQ to the external medium to initiate the 1-min uptake measurements, which in our assays reflected the maximal transport activity (17).

The highly PPQ-R Dd2 + F145I isoform had the highest PPQ uptake activity, followed closely by Dd2 + F145I + F131C and Dd2 + F145I + I347T (Fig. 2D). These similar levels of PPQ uptake contrast with differences in the PPQ susceptibility of these two lines *in vitro* (Fig. 2B). Prior work has shown that isoforms with different PPQ resistance levels can transport this drug at similar levels in this assay format (16), suggesting a concentration-dependent mechanism of transport. Dd2 + F145I + C258W had reduced PPQ uptake, equal to half the level of Dd2 + F145I and consistent with the former isoform not conferring PPQ resistance. The 3D7 isoform demonstrated negligible transport at 100 nM ^{3}H-PPQ, whereas the Dd2 isoform displayed low levels of transport at this PPQ concentration. This observation showed some contrast with the finding that parasites expressing either 3D7 or Dd2 PfCRT were PPQ-sensitive.

The CQ uptake data were more consistent with parasite susceptibility profiles (Fig. 2C and E; Table S3). The CQ-resistant Dd2 and the WT 3D7 isoforms exhibited the highest and lowest levels of CQ uptake, respectively. Dd2 + F145I PfCRT displayed reduced CQ transport, in agreement with the sensitization of Dd2$^{Dd2+F145I}$ parasites to CQ. The Dd2 +

F145I + F131C and Dd2 + F145I + I347T isoforms had a slight but insignificant increase in CQ uptake, concordant with parasite IC_{90} data. Dd2 + F145I + C258W PfCRT-containing liposomes accumulated the highest levels of CQ compared to Dd2 + F145I, although these were less than Dd2. As seen in other PfCRT transport studies, the 3D7 isoform had low levels of CQ transport, notwithstanding the sensitivity of WT parasites (31). These variations in PPQ and CQ transport likely reflect the differential involvement of these mutated amino acids in PfCRT-mediated drug transport. Of these four mutations, only F145I faces the inner cavity through which drug is transported (Fig. S4), which leads us to speculate that the other three mutations likely alter protein conformation to impact PPQ and/or CQ transport.

Molecular dynamics energy minimization calculations provide evidence of conformational changes that would impact PfCRT interactions with drugs

Subsequently, we used Monte Carlo Energy Minimization Molecular Dynamics to predict how the individual amino acid substitutions found in the three novel PfCRT isoforms might perturb local protein structure and drug interactions (32). As expected, the structures of the four PfCRT isoforms studied herein (Dd2 + F145I, Dd2 + F145I + F131C, Dd2 + F145I + C258W, and Dd2 + F145I + I347T) shared many similarities with the CQ-resistant Dd2 isoform from which they were derived (Fig. 3A and B). Nonetheless, the minor local differences between isoforms provide insight into their different PPQ binding or transport properties (PPQ is similar in structure to a CQ "dimer"), relative to CQ (18). To identify local differences in structure that may be relevant for the altered parasite phenotypes mediated by these novel PfCRT isoforms, we performed molecular dynamics analyses, as earlier applied to PfCRT to inventory residue side chain-side chain hydrogen bonds (HB) and salt bridges (SB) (32). Key differences between the isoforms are summarized in Table 2 with a full inventory of SB provided in Table S4.

Notably, all four isoforms lost key interactions within the "K76 region" that helps define drug binding site B, previously identified for the CQ-resistant Dd2 PfCRT (32). These include important Y68-D329 and H97-S326 HB present for Dd2 PfCRT but either absent or reduced to a minor contribution for all other isoforms, respectively (Table 2). In addition, three SB near the interface of the PfCRT three-helical "zipper" and the cytosolic end of the putative drug cavity are lost for all F145I mutant isoforms (Fig. S5). The F145I substitution in Dd2 PfCRT removed a phenyl aromatic ring (F145) that normally rests between drug binding sites A (at the entrance of the central cavity) and B (within this cavity about three helical turns away from site A). With F145, the ring is positioned directly within the cavity within ~7 Å of drug bound within site A (Fig. 3C) and is capable of π-π interactions with the CQ or PPQ quinoline ring during drug transit from site A to site B, whereas the alkyl side chain in 145I is not, likely influencing the energetics of the transition of CQ and PPQ drugs between the two binding sites.

Lastly, we observed an extended three-ring π-π stabilizing interaction for Dd2 PfCRT (Fig. 3D), which was conspicuously absent in the Dd2 + F145I + F131C isoform. Similar to the SB disruptions that appear to destabilize interactions between the cytosolic entrance to the PfCRT central cavity and the three-helix bundled PfCRT "zipper" noted earlier, the predicted loss of three-ring π-π interactions between residues 131, 251, and 252 likely perturbs binding of the zipper bundle to the cytosolic rim of the drug cavity. These simulations predict altered release of CQ and PPQ in these novel PfCRT isoforms relative to Dd2 PfCRT.

Dd2 + F145I + C258W PfCRT results in decreased accumulation of short Hb-derived peptides in the DV

Recent studies have linked PPQ resistance with excess accumulation of peptides resulting from aberrant Hb digestion and peptide processing in PfCRT mutants, including $Dd2^{Dd2+F145I}$ (21). This is believed to modify DV physiology and affect access to amino acids for protein synthesis and intra-erythrocytic development. Given the increase in parasite fitness and alteration in DV size in our mutated F145I lines, we hypothesized that

these novel PfCRT mutations may alleviate, to varying degrees, the buildup of peptides in this organelle. Peptidomic analysis, using liquid chromatography–mass spectrometry (LC-MS) revealed a total of 134 putative endogenous Hb-derived peptides, differing in both charge and length, identified in one or more samples (Table S5). We observed higher levels of peptides in $Dd2^{Dd2+F145I}$ parasites compared to $Dd2^{Dd2}$ (Fig. 4A), consistent with earlier findings (21). To determine the effect of the secondary mutations on peptide levels, each of the lines was compared to $Dd2^{Dd2+F145I}$. Parasites harboring the F131C or I347T PfCRT mutations added to Dd2 + F145I accumulated slightly increased levels of short peptides (mostly two to five amino acids in length), exhibiting a similar phenotype to $Dd2^{Dd2+F145I}$ (Fig. 4A). The $Dd2^{Dd2+F145I+C258W}$ line, however, had markedly diminished levels of short peptides with over 75% of peptides decreased compared to $Dd2^{Dd2+F145I}$ (Fig. 4A). We identified 27, 1, 8, and 31 differentially accumulated peptides in $Dd2^{Dd2}$, $Dd2^{Dd2+F145I+F131C}$, $Dd2^{Dd2+F145I+I347T}$, and $Dd2^{Dd2+F145I+C258W}$, respectively, which differed

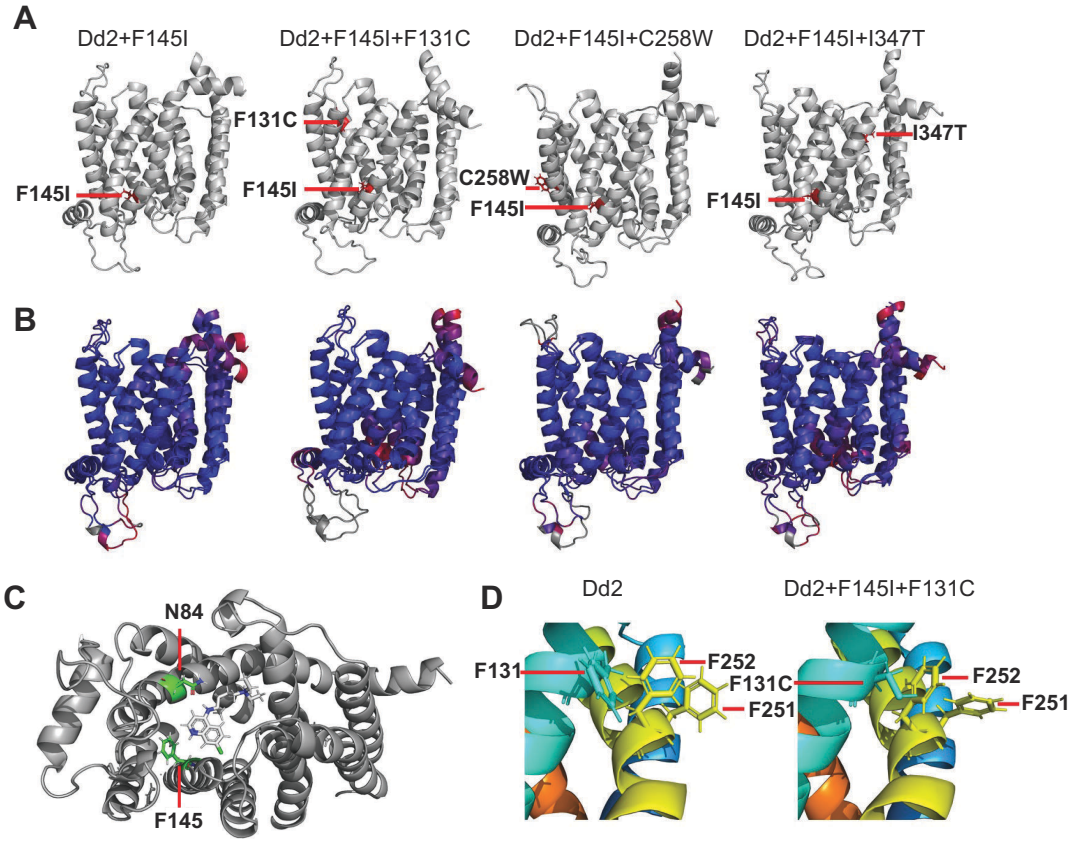

FIG 3 Molecular dynamics of the various PfCRT isoforms in this study. (A) Average energy minimized from cryoEM template (EMMD; see reference 32) structures of Dd2 + F145I, Dd2 + F145I + F131C, Dd2 + F145I + C258W, and Dd2 + F145I + I347T, with mutations highlighted relative to Dd2. (B) Root mean square deviation (RMSD) comparison of Dd2 PfCRT EMMD (32) vs Dd2 + F145I, Dd2 + F145I + F131C, Dd2 + F145I + C258W, or Dd2 + F145I + I347T EMMD structures (from left to right). Differences are highlighted using ColorByRMSD where blue indicates minimum RMSD and red indicates maximum RMSD. Gray regions were not compared. The structures are all highly similar with minimum RMSDs (0.18, 0.41, 0.11, and 0.39 Å from left to right), low average RMSDs (2.22, 2.44, 1.81, and 2.54 Å from left to right), and small regions of maximum RMSDs (11.91, 10.42, 9.44, and 9.73 Å from left to right) corresponding to particularly flexible PfCRT domains. (C) The previously proposed CQ binding site A in Dd2 showed direct interactions between the anilinyl CQ nitrogen (middle blue on the CQ molecule) and the oxygen of N84 (red) that is ~3.2 Å away. F145, positioned directly between the proposed CQ binding sites A and B, is likely to interact with the drug's quinolinyl ring throughπ-π interactions during transit between the two sites. Notably, these π-π interactions were predicted to disappear upon mutation to isoleucine (F145I). The distance between the drug quinolinyl and F145 phenyl rings in site A is 7.4 Å. (D) The predicted three-phenylalanine π-π bundle for Dd2 PfCRT formed between the side chains of F131, F251, and F252 near the cytosolic ends of helices 3 (aqua) and 7 (yellow-green), respectively, is lost in the Dd2 + F131C + F145I isoform.

TABLE 2 PfCRT isoform interactions[a]

	Interaction	Residue 1	Residue 2
All five isoforms	D57/K53	JM1	JM1
	E54/R392	JM1	TM10
	D311/K85	L7	L1
	E204/K200	L5	TM5
	D377/R374	TM10	L9
	E399/R392	TM10	TM10
Dd2 and Dd2 + F145I	D313/K317	L7	TM8
Dd2 only	D137/R231	TM3	TM6
	E232/K236	TM6	TM6
	D338/K339	TM8	TM8
	Y68/D329	TM1	TM8
	H97/S326*	TM2	TM8

[a]List of interactions discussed in this study. HB are in boldface; SB are not. The interaction between H97 and S326 is present in all isoforms (*) but present for substantially less time for all F145I mutant isoforms relative to Dd2 PfCRT (≤30% vs 86% of simulation time).

significantly from those in $Dd2^{Dd2+F145I}$ ($P \geq 0.05$ in unpaired *t*-tests; Fig. 4B and C; Table S6). Only five of the 27 peptides whose levels were altered in $Dd2^{Dd2}$ were also increased in $Dd2^{Dd2+F145I+C258W}$, suggesting that the C258W mutation alleviated peptide defects imparted by F145I, restoring regular peptide homeostasis (Fig. S6). Strikingly, all of the peptides with altered levels in $Dd2^{Dd2+F145I+C258W}$ were reduced in abundance, which may explain the gain of fitness in this line relative to $Dd2^{Dd2+F145I}$. Differentially accumulated peptides were typically two to four amino acids in length (Fig. 4B), had isoelectric points of three to six (Fig. 4C), and were neutral or carried a single negative charge at pH values of 5.5 or 7.4 (reflecting conditions in the DV lumen or cytosolic conditions, respectively) (Fig. S7), in accordance with prior studies (21, 33).

We used our proteoliposome system to explore whether peptides could compete for mutant PfCRT-mediated drug transport. These assays utilized the purified recombinant 7G8 + F145I and 7G8 isoforms, which mediate transport of ^{3}H-PPQ and ^{3}H-CQ, respectively (17). Assays focused on HVDDM and VDPVNF, as truncated or elongated versions of these peptides showed differences in $Dd2^{Dd2}$ and $Dd2^{Dd2+F145I+C258W}$, respectively, relative to $Dd2^{Dd2+F145I}$ (Table S6). These two peptides were also previously found to inhibit ^{3}H-CQ transport via Dd2 PfCRT expressed on the surface of *Xenopus* oocytes (34), and truncated versions were earlier reported to differ in their levels when comparing $Dd2^{Dd2}$ with $Dd2^{Dd2+F145I}$ (21). Both peptides showed substantial inhibition of ^{3}H-PPQ or ^{3}H-CQ transport, to levels similar to competitive inhibition with non-labeled PPQ or CQ (Fig. S8). Control assays showed no competition with pyrimethamine or atovaquone, unrelated drugs that are known to not interact with PfCRT.

DISCUSSION

In this study, we characterized novel PfCRT mutations that emerged on the PPQ-R Dd2 + F145I PfCRT isoform—both with cultured parasites (F131C and I347T) and in SE Asian field isolates (C258W). Each of these mutations alleviated the fitness cost of Dd2 + F145I PfCRT to varying degrees and likely evolved to increase parasite replication rates in the absence of drug pressure. Both the C258W and I347T variants displayed reduced PPQ resistance, with the former being detected in SE Asia following the removal of PPQ as a first-line partner drug (27). Notably, the C258W field mutation restored CQ resistance to levels seen in Dd2 parasites, in contrast with the two mutations obtained during extended *in vitro* culture that conferred hypersensitization to CQ and md-CQ. Biochemical assays with purified PfCRT protein and peptidomic analysis revealed mechanistic differences that affect drug susceptibility, intracellular peptide availability, and parasite fitness.

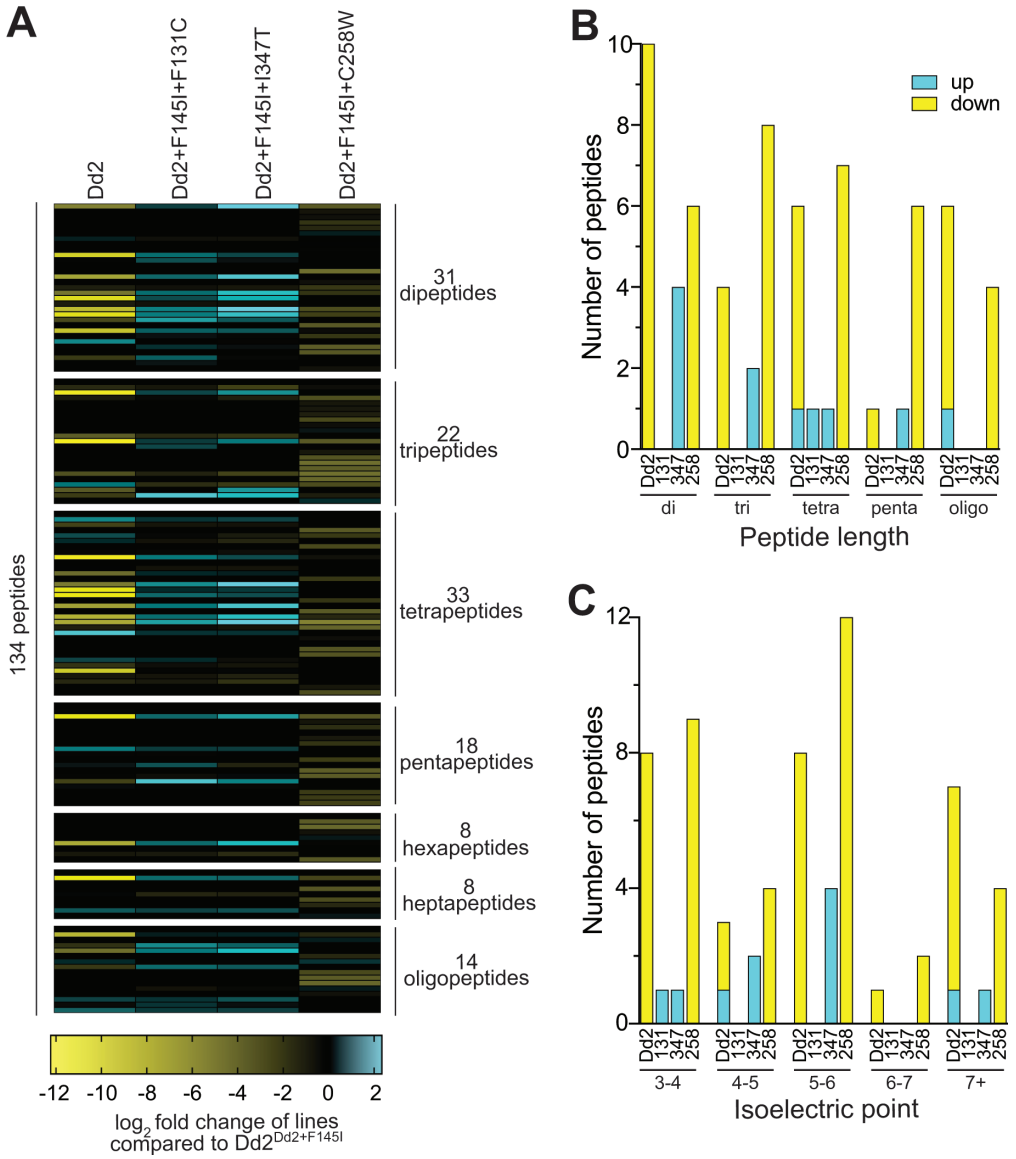

FIG 4 $Dd2^{Dd2+F145I+C258W}$ results in decreased accumulation of peptides. (A) Heatmap of 134 peptides (detected in positive or negative modes and present in metabolite extracts from any of the parasite lines) classified by peptide length. These data are presented as the $\log_2$ fold change in the average abundance of each peptide identified compared to $Dd2^{Dd2+F145I}$. N = 3; n = 3. Oligo refers to peptides eight or more amino acids in length. PfCRT haplotypes of the isogenic lines are listed. (B and C) Significant differences in peptide levels between lines with a given mutation and Dd2 + F145I are shown ($P < 0.05$ in unpaired *t*-tests). Peptides are classified by (B) peptide length or (C) isoelectric point. Details are provided in Tables S4 and S5.

Our data highlight the interplay between resistance, fitness, and drug usage that can impact which parasite genotypes predominate in individual regions. The introduction of DHA-PPQ in the late 2000s in Cambodia is known to have selected for novel PfCRT mutations, including F145I, in parasites expressing the CQ-resistant Dd2 isoform. These mutations have been shown to confer PPQ resistance *in vitro* and have been associated with an increased risk of treatment failure (9, 11, 12, 14, 35). Evidence suggests that F145I, which was among the earliest mutations and mediates high level resistance, was later replaced by the T93S, H97Y, and I218F mutations that, while less resistant, showed a smaller fitness cost (13, 15). These findings lead us to speculate that the emergence of the C258W mutation in the field and F131C and I347T in cultured parasites was a result primarily of improved fitness driving faster propagation rates (Fig. 1). As has been seen

with CQ resistance, even a marginal increase in growth rate per generation can allow a parasite strain to gain prevalence. Earlier studies in Malawi have shown that the fitness costs observed with CQ-resistant PfCRT isoforms was sufficient for WT, CQ-sensitive parasites to quickly overtake mutant lines in the absence of CQ usage in clinics (36, 37). Recent data from the MalariaGEN Pf7 genome study provide evidence of a similar trajectory with mutant PfCRT in SE Asia, as the parasite evolves away from PPQ-R PfCRT isoforms that impart a substantial fitness cost (27).

The identification of distinct mutations in the field and in lab-cultured parasites suggests multiple evolutionary paths for PfCRT. We observed a range of PPQ phenotypes with our original clones and edited lines that inversely correlated with growth rate, i.e., the more resistant parasites displayed a stronger fitness cost (Fig. 1B and Fig. 2A). The F131C mutants maintained high survival rates in the PSA with only a small improvement in growth rate per generation compared to $Dd2^{Dd2+F145I}$ (~2%), whereas the I347T parasite lines became fully sensitized to PPQ but had up to a twofold increase in replication rate. The C258W variant had a more moderate increase in fitness despite a complete loss of PPQ resistance, as evidenced by decreased PSA and PPQ IC_{90} values. These data illustrate the often dichotomous relationship between parasite fitness and increased PSA survival rates (38). Observations from these edited lines may provide lessons on the evolution of the SE Asian parasite landscape after DHA-PPQ cessation, pointing to a rapid loss of resistance. These data also underscore the necessity for routine surveillance of the entire *pfcrt* locus. Importantly, the presence of the F145I point mutation does not guarantee PPQ resistance.

Strikingly, Dd2 + F145I + C258W PfCRT mediates CQ resistance, despite the presence of the F145I mutation and lack of CQ pressure in SE Asia (Fig. 2C). PPQ-R mutations, which line the drug-transporting central cavity of PfCRT, generally hypersensitize the parasite to CQ (12). The C258W mutation faces away from this cavity (Fig. S4), potentially causing a conformational change that affects both PPQ and CQ transport. The elevated CQ IC_{90} of this field line is important to note given the recent modeling data suggesting that simultaneous administration of PPQ and CQ could preclude the acquisition of dual drug resistance (16). Critically, there was no change in parasite susceptibility to MFQ, the first-line ACT partner drug in Cambodia, in any of the mutant lines (Fig. S3F).

Our transport studies with purified PfCRT variants reveal notable differences between CQ and PPQ, despite these both being 4-aminoquinoline compounds (PPQ is a bis-4-aminoquinoline with two CQ-like structures connected by a central linker). For CQ, transport levels were consistent with the CQ inhibitory values against resistant and sensitive parasite lines, highlighting drug efflux as the primary determinant of resistance (Fig. 2C and E) (39). For PPQ, however, transport and susceptibility data do not match as closely. At 100 nM ^{3}H-PPQ, the Dd2 + F145I, Dd2 + F145I + F131C, and Dd2 + F145I + I347T isoforms transported comparable amounts of drug, despite the PPQ-sensitive phenotype of the I347T variant (Fig. 2B and D). This difference has also been observed with ^{3}H-CQ and ^{3}H-PPQ cellular accumulation studies in the parasite (17). One possible explanation for the differences in CQ and PPQ transport could be due to the increased protonation state of PPQ. Inside the DV (whose pH is estimated to be ~5.2 40]), CQ would be protonated at both its nitrogens, whereas PPQ can have up to four protonated nitrogens. CQ transport via mutant PfCRT was earlier shown to be dependent on H^+ co-transport (41). We speculate that, once PPQ reaches a certain concentration in the DV, there may be sufficient protons to permit efficient transport without requiring external protons. In the parasite, PPQ resistance is evident only at high concentrations of drug, manifesting at the IC_{90} but not IC_{50} level. One caveat of our study is that transport measurements were conducted at a single concentration (100 nM ^{3}H-PPQ). A recent study observed growth inhibition of PfCRT-expressing *Saccharomyces cerevisiae* yeast only at levels of 300 µM PPQ as a surrogate of transport measurement (18). Technical considerations preclude using high concentrations of ^{3}H-PPQ in our assays.

Molecular dynamics simulations uncovered subtle differences between isoforms that were predicted to result in the loss of several key molecular interactions in the central

cavity of PfCRT (Fig. 3). This includes the loss of SB involving residues on TM3, TM6, and TM8 near the cytosolic entrance of the central drug-binding cavity, likely providing greater helical flexibility to facilitate release of the larger PPQ molecule as opposed to the smaller CQ (32). Also, another perturbation involves residue 131 (i.e., the mutated amino acid in the PPQ-R Dd2 + F145I + F131C). Previous molecular dynamics studies have suggested that the F145I mutation induces a conformational change in PfCRT, attributing PPQ resistance to these structural alterations as opposed to changes in electrostatic properties (16, 17). Our study now predicts the disappearance of π-π interactions with PPQ upon the replacement of the aromatic phenylalanine with isoleucine. These molecular dynamics simulations support the hypothesis that CQ and PPQ binding within PfCRT involves different side chain interactions and conformations of the protein (19) and predict that a given point mutation can lead to small changes in structure that result in larger changes in drug susceptibility phenotypes.

In previous metabolomic analyses, $Dd2^{Dd2+F145I}$ accumulated high levels of Hb-derived peptides (21), a phenotype that was replicated in our study. Given this, we hypothesized that the physiological rationale for acquiring second-site mutations may be to alleviate this buildup of peptides. This was true for the $Dd2^{Dd2+F145I+C258W}$ line, with the majority of Hb-derived peptides showing relatively reduced abundance (Fig. 4A). Among the 31 peptides that showed a significant decrease compared to $Dd2^{Dd2+F145I}$ (Fig. 4B and C; Table S6), we observed PVNF and HVDD, as well as the dipeptides VG, GV, NP, and PA, which have been identified in earlier PfCRT studies (21, 34). PfCRT is thought to transport Hb-derived peptides from the DV lumen to the cytosol (34). It is possible that the C258W mutation emerged in field isolates to correct impaired peptide efflux by Dd2 + F145I PfCRT, thereby increasing amino acid availability in the cytosol and improving parasite replication rates (42). We note that most of the previously identified peptides were short (4–11 amino acids in length) and were neutral or had a single positive charge, in accordance with the increased pool of peptides in the $Dd2^{Dd2+F145I+C258W}$ line. In addition, this excess of peptides in the DV likely causes bloating of this organelle, as exhibited by $Dd2^{Dd2+F145I}$ but not $Dd2^{Dd2+F145I+C258W}$ (Fig. S2), which we suspect might lead to increased osmotic pressure and decreased proliferative potential.

Interestingly, quantitative peptidomics did not reveal a major difference in peptide accumulation in $Dd2^{Dd2+F145I+F131C}$ and $Dd2^{Dd2+F145I+I347T}$ relative to $Dd2^{Dd2+F145I}$, with only one or eight peptides significantly altered in these lines, respectively (Fig. 4B and C; Table S6). In both lines, schizonts still had bloated vacuoles, further confirming a buildup of peptides in the DV (Fig. S2). A reduced accumulation of short peptides, however, may not fully explain the gain in fitness in these parasites. PfCRT mutations have also been associated with defective Hb catabolism and alterations in ionic balance (21, 43), which may impact fitness. Further studies on these lines will be necessary to determine additional physiological effects of these mutations and how they alter ABS parasite fitness.

Our data underscore how changes in parasite fitness and antimalarial susceptibility can drive parasite genetic evolution in endemic areas with differing drug selective pressures. PPQ-R parasites appear to be highly transient in the absence of sustained PPQ pressure, due to the large fitness cost of their mutations. Reduced fitness has also been implicated with multicopy *plasmepsin II/III* that co-evolved with PPQ-R PfCRT isoforms in the field and that appear to augment resistance (13, 26). In light of these data, DHA-PPQ may be a good candidate as part of a multiple first-line therapy strategy (i.e., used simultaneously with a separate ACT) in SE Asia to delay the emergence of resistance (44–47). Nonetheless, as different drug regimens are implemented in SE Asia, it will be imperative to survey the entire *pfcrt* allele to ascertain resistance status, as the presence of a single point mutation does not guarantee resistance to PPQ or sensitivity to CQ.

MATERIALS AND METHODS

Whole-genome sequencing

Sequencing of genomic DNA from mutant and parental lines employed an Illumina TruSeq DNA PCR-Free library preparation protocol and a MiSeq sequencing platform, as described (48). The list of variants was compared against the Dd2 +F145I parent to obtain homozygous SNPs that were present exclusively in the clones.

Plasmid construction, parasite culturing, and transfections

pfcrt was edited using customized zinc finger nucleases and a two-plasmid approach that replaces the endogenous allele with a recombinant allele containing the mutations of interest (28). Mutations were introduced into a *pfcrt*^{Dd2} donor plasmid by site-directed mutagenesis (Fig. S1 and Table S7). Dd2 *P. falciparum* ABS parasites were cultured in human O$^+$ red blood cells (RBCs) in RPMI 1640-based culture media containing 0.5% (wt/vol) Albumax (49). RBCs were purchased from the Interstate Blood Bank (Memphis, TN) as pooled, de-identified, anonymized blood that was washed to remove any residual leukocytes. Approval for this protocol (AAAU3761) was provided on 28 October 2022 by the Columbia University Institutional Review Board, which deemed this work to be Not Human Subjects Research Under 45 CFR 46.

Parasites were cultured at 37°C in an airtight chamber with 5% O_2/5% CO_2/90% N_2. Ring-stage parasites were electroporated with 50–100 µg of purified plasmid DNA in Cytomix (49). The donor plasmid carrying the human *dhfr* marker was selected with 2.5 nM WR99210 (Jacobus Pharmaceuticals), and the zinc finger nuclease plasmid expressing blasticidin S-deaminase was selected with a 6-day pulse of 2 µg/mL blasticidin hydrochloride (Thermo Fisher). Editing was confirmed using PCR primers p1–7 (Fig. S1; Table S7) and Sanger sequencing, and clones were obtained by limiting dilution.

In vitro fitness assays

We measured relative growth rates of *pfcrt*-edited parasite lines using *in vitro* competition assays (10, 12). Briefly, parasites were co-cultured in 96-well plates in a 1:1 ratio with a Dd2 reporter parasite line (termed Dd2-GFP) that expresses eGFP (24). Parasites were stained with MitoTracker Deep Red and growth monitored for 21 days on an iQue flow cytometer. Relative growth rates of each test line are shown by plotting the percentage of GFP$^+$ cells in culture over time. The fitness cost associated with a line expressing a given PfCRT mutation was calculated relative to the Dd2 GFP$^+$ reporter line using the following formula: $P' = P[(1 - x)^n]$, where P' is equal to the parasitemia at the assay endpoint, P is equal to the parasitemia on day 0, n is equal to the number of generations from the assay start to finish, and x is equal to the fitness cost (50). This equation assumes 100% growth for the GFP$^+$ comparator line. The assay endpoint was defined as the final day of the experiment day 21, resulting in the number of parasite generations (n) being set to 10.5. From these data, we determined the fitness cost relative to Dd2^{Dd2}.

Piperaquine survival assay

For PSAs, we seeded tightly sorbitol-synchronized ring-stage parasites (0–6 h post invasion) at 1% parasitemia and 1% hematocrit in 96-well flat-bottom plates containing 10-point, twofold dilutions with a maximum of 1,600 nM PPQ (12, 13, 30). Parasites were incubated for 72 h at 37°C. Parasites were labeled with SYBR Green I and MitoTracker Deep Red (as DNA and mitochondrial dyes, respectively), and parasitemias were measured on an iQue Plus flow cytometer. Percent survival was calculated by dividing the parasitemia of the PPQ-treated parasites by that of the no-drug control (10, 12). Statistical significance was determined using non-parametric Mann-Whitney U tests (GraphPad Prism 8 software). Raw data and statistics are listed in Table S1.

Drug susceptibility assays

Asynchronous, ABS parasites were plated at 0.3%–0.5% parasitemia and 1% hematocrit in 96-well plates and incubated with a 10-point, twofold range of drug concentrations. Plates were incubated at 37°C for 72 h, and parasitemias were measured by flow cytometry. IC_{50} values were calculated by nonlinear regression analysis. Statistical significance was determined using Mann-Whitney *U* tests (Table S2).

PfCRT protein expression and purification

The *pfcrt* full-length open-reading frames were cloned into the pEG BacMam vector (51), and recombinant P3 baculovirus was prepared as described in reference 17. Proteins were expressed in HEK293S GnTi-negative cells and purified by Ni^{2+}-NTA resin chromatography (17, 52).

Transport assays

Purified PfCRT variants were reconstituted in preformed liposomes (composed of *E. coli* total lipids:CHS at a ratio of 94:6 [wt/wt] and a protein:lipid ratio of 1:150 [wt/wt]). Each uptake assay was performed with 50 ng of PfCRT in proteoliposomes, and 1-min uptakes of ^{3}H-CQ (50–100 nM, 1 Ci/mmol) or ^{3}H-PPQ (50–100 nM, 1 Ci/mmol; both from American Radiolabeled Chemicals, Inc.) were performed as described (17). Statistical significance was determined using Mann-Whitney *U* tests (Table S3).

Simulations of molecular dynamics

Monte Carlo Molecular Dynamics (MC/MD) energy minimization computations for the PfCRT Dd2 isoform have been published previously (32). MC/MD energy minimization for the four additional PfCRT protein isoforms analyzed here (Dd2 + F145I, Dd2 + F145I + F131C, Dd2 + F145I + C258W, and Dd2 + F145I + I347T) was performed essentially as described previously for Dd2. In brief, we first imported the structure of the PfCRT Dd2 isoform solved by mutagenesis and MC/MD methods, based on the 7G8 PfCRT isoform cryo-EM structure template (PDB code: 6UKJ), into Maestro (53). The additional PfCRT isoforms (Dd2 + F145I, Dd2 + F145I + F131C, Dd2 + F145I + C258W, and Dd2 + F145I + I347T) were generated using Maestro's Residue and Loop Mutation tool. Each isoform was then prepared using Protein Preparation Wizard to bond orders. We added missing hydrogen atoms using Prime Protonation states of ionizable residues, fixed at pH 5.0 (near the pH of the DV), using ProtAssign. Each isoform was embedded within a 1-palmitoyl-2-oleoyl-sn-glycero-3-phosphocholine (POPC) membrane (54). Boundary conditions were an orthorhombic box expanding 10 Å beyond the protein in the X, Y, and Z dimensions (membrane defines the X,Y plane), solvated with simple point-charge water, and neutralized with chloride ions. MC/MD simulations each lasted 10 ns (55). Three independent simulations were done for each isoform and then averaged before analysis and comparison to Dd2 PfCRT. Each calculation began with default relaxation followed by simulation in an isothermal, isobaric NPT ensemble with constant particle number (N), pressure (P; 1.01325 bar), and temperature (T; 310 K) (32). Convergence for each simulation was typically observed within 2–4 ns.

To analyze isoforms, clusters were created for each MC/MD trial and combined, and all atoms then included as the root mean square deviation (RMSD) matrix. Clustering was with the Desmond Trajectory Clustering tool (56), and water and POPC membrane were manually removed with Maestro for ease of visual comparison. To compare PfCRT isoforms, all-atom RMSD was generated, and local structural differences were visualized using PyMOL ColorByRMSD (57). SB and side chain-side chain HB differences were identified using Visual Molecular Dynamics (VMD) software (58) as described (32). After scanning the entire protein, HB were defined as hetero-atom distances within 3.2 Å with bond angle 180° ± 45°, and SB, as hetero-atom interactions used a cutoff of 4 Å. Heatmaps summarizing pair interaction were generated using VMD.

Sample preparation for untargeted LC-MS metabolomics

Mycoplasma-free parasites were synchronized to trophozoites using sorbitol, followed by MACS CS columns on a SuperMACS II Separator (Miltenyi Biotec) to remove uninfected RBCs. Hydrophilic parasite metabolites were extracted using 1-mL 90% cold methanol with 0.5 µM [$^{13}C_4$, $^{15}N_1$]-aspartate (Cambridge Isotope Laboratories) as the internal standard to correct for technical variations arising from sample processing. Cell pellets were disrupted by thoroughly vortexing the sample tubes, the insoluble debris was pelleted by centrifugation (13,000 × *g*, 10 min), and the supernatant was collected and dried down under nitrogen gas flow. Samples were then resuspended in HPLC-grade water containing 1 µM chlorpropamide (Alpha Aesar) as an internal standard to correct for signal deviation due to instrument variance. A quality control sample consisting of all samples pooled together was created and periodically measured throughout the run to monitor signal consistency throughout the otherwise randomized run order.

LC-MS parameters and methods

Five microliters of each sample were injected for analysis. Metabolites were analyzed using a reversed phase method on an HPLC Prominence 20 UFLCXR system (Shimadzu) with a Waters BEH C18 column (100 mm × 2.1 mm, 1.7-µm particle size) at 55°C and an aqueous acetonitrile gradient run for 20 min at a flow rate of 250 µL/min. Solvent A was an HPLC-grade water with 0.1% formic acid, and solvent B was an HPLC-grade acetonitrile with 0.1% formic acid. The solvent gradient was as follows: at 0.0 min, 3% of B; 10.0 min, 45% of B; 12.0 min, 75% of B; 17.5 min, 75% of B; and 18.0–20.0 min, 3% of B. Eluate was delivered into a (QTOF) 5600 TripleTOF using a DuoSpray ion source (AB Sciex). Capillary voltage was 5.5 kV in positive and 3.8 kV in negative ion mode with declustering potentials of 80 V and −80 V, respectively. During the analysis, curtain gas pressure of 25 psi, nebulizer gas (GS1) of 50 psi, heater gas 2 (GS2) of 50, and heater temperature of 600°C were applied. The TripleTOF was scanning 50 to 1,000 m/z, and 16 MS/MS product ion scans (100 ms) per duty cycle using collision energy of 50 V with a 20-V spread.

Data analyses for metabolomics

Analyses were performed as previously described (21). The labeled [$^{13}C_4$, $^{15}N_1$]-aspartate internal standard intensity was assessed for technical reproducibility. Peak areas from both positive and negative modes were exported, and the resulting feature quantification matrices were used as input for a custom R script designed to putatively annotate peak groups as human Hb-derived peptides of matching m/z value within 15 ppm, considering all potential human Hb peptides up to 13 amino acids long. Peak areas from both positive and negative modes were exported for downstream analysis. The chlorpropamide standard was used as an internal control to normalize individual metabolite peak areas between runs. The peak areas for duplicate metabolites were summed before blank subtraction. Peak areas of the blanks were subtracted from the samples for each metabolite and in each experiment. The relative standard deviation of quality controls was tested, and only peptides with a value <30 were retained. The isoelectric point and charge at pH 5.5 and pH 7.4 for each oligopeptide were calculated using the web-based isoelectric point calculator IPC2.0 (59). Data from three independent experiments, each with three technical replicates, were averaged. To investigate the effect of PPQ-R PfCRT mutations on *P. falciparum* metabolism, the $\log_2$ fold changes of mutant vs Dd2$^{Dd2+F145I}$ metabolites were calculated for each experimental run using the averaged replicate peak areas. Raw data are listed in Table S5. The Venn diagram in Fig. S6 was made using the website http://bioinformatics.psb.ugent.be/webtools/Venn/.

ACKNOWLEDGMENTS

We express our gratitude to Dr. Olivo Miotto (Nuffield Department of Medicine, Oxford, UK) for his support and feedback. We also would like to thank Dr. Brian Kloss and Dr.

Renato Bruni at the New York Structural Biology Center (New York Structural Biology Center) for generating recombinant baculovirus for protein expression. We gratefully acknowledge Dr. Anne-Catrin Uhlemann (Director, Columbia University Microbiome and Pathogen Genomics Core) for whole-genome sequencing and Dr. Sachel Mok (Columbia University Irving Medical Center) for her kind help in providing a protocol for metabolomic analysis. We also thank the Huck Institutes of Life Sciences Metabolomics Core Facility at Penn State University.

Partial funding for this work was provided by the NIH (R01 AI050234, R01 AI124678, and R21 AI159558 to D.A.F.; R01 AI147628 to F.M., M.Q., and D.A.F.; F31 AI157410 to L.M.H.; RO1 AI056312, R21 AI146506, and R21 AI168720 to P.D.R.; and K08 AI163497 to J.L.S.-S.). L.M.H. also acknowledges support from the Columbia University Graduate Program in Microbiology and Immunology (NIH T32 AI106711). J.L.S.-S. was also supported by a Doris Duke Physician Scientist award (DDCF Grant 2019121) and a Louis V. Gerstner, Jr. Award. G.W.R. is supported by the Pennsylvania State University Eberly College Postdoctoral Research Fellowship.

L.M.H., S.K.D., and D.A.F. conceived and designed the study. L.M.H., S.K.D., J.L.S.-S., K.A.S., T.Q., G.W.R., E.G.-I., J.K., J.O., A.W., P.D.R., and T.Y. acquired and analyzed the data. L.M.H. and D.A.F. wrote the manuscript, with input from all authors.

AUTHOR AFFILIATIONS

[1]Department of Microbiology and Immunology, Columbia University Irving Medical Center, New York, New York, USA
[2]Center for Malaria Therapeutics and Antimicrobial Resistance, Columbia University Irving Medical Center, New York, New York, USA
[3]Division of Infectious Diseases, Department of Medicine, Columbia University Irving Medical Center, New York, New York, USA
[4]Department of Chemistry, Pennsylvania State University, University Park, Pennsylvania, USA
[5]Department of Biochemistry and Molecular Biology and Huck Center for Malaria Research, Pennsylvania State University, University Park, Pennsylvania, USA
[6]Department of Chemistry, Georgetown University, Washington, DC, USA
[7]Department of Biochemistry and Cellular and Molecular Biology, Georgetown University, Washington, DC, USA
[8]Department of Psychiatry, Columbia University Irving Medical Center, New York, New York, USA
[9]Department of Physiology and Cellular Biophysics, Columbia University Irving Medical Center, New York, New York, USA
[10]Area Neuroscience - Molecular Therapeutics, New York State Psychiatric Institute, New York, New York, USA

AUTHOR ORCIDs

Laura M. Hagenah http://orcid.org/0000-0001-8258-6823
Jennifer L. Small-Saunders http://orcid.org/0000-0001-6064-2249
Manuel Llinás http://orcid.org/0000-0002-6173-5882
David A. Fidock http://orcid.org/0000-0001-6753-8938

FUNDING

Funder	Grant(s)	Author(s)
HHS | NIH | National Institute of Allergy and Infectious Diseases (NIAID)	R01 AI050234, R01 AI124678, R21 AI159558	David A. Fidock
HHS | NIH | National Institute of Allergy and Infectious Diseases (NIAID)	R01 AI147628	Filippo Mancia

Funder	Grant(s)	Author(s)
HHS | NIH | National Institute of Allergy and Infectious Diseases (NIAID)	F31 AI157410	Laura M. Hagenah
HHS | NIH | National Institute of Allergy and Infectious Diseases (NIAID)	K08 AI163497	Jennifer L. Small-Saunders
HHS | NIH | National Institute of Allergy and Infectious Diseases (NIAID)	T32 AI106711	Laura M. Hagenah
Doris Duke Charitable Foundation (DDCF)	2019121	Jennifer L. Small-Saunders
Gerstner Family Foundation		Jennifer L. Small-Saunders
HHS | NIH | National Institute of Allergy and Infectious Diseases (NIAID)	R01 AI056312, R21 AI146506, R21 AI168720	Paul D. Roepe

AUTHOR CONTRIBUTIONS

Laura M. Hagenah, Conceptualization, Data curation, Formal analysis, Investigation, Methodology, Validation, Writing – original draft, Writing – review and editing | Satish K. Dhingra, Conceptualization, Investigation, Methodology | Jennifer L. Small-Saunders, Investigation | Tarrick Qahash, Formal analysis, Investigation | Andreas Willems, Investigation, Visualization, Writing – review and editing | Kyra A. Schindler, Investigation | Gabriel W. Rangel, Formal analysis, Investigation | Eva Gil-Iturbe, Formal analysis, Investigation | Jonathan Kim, Investigation | Emiliya Akhundova, Investigation | Tomas Yeo, Formal analysis | John Okombo, Investigation | Filippo Mancia, Funding acquisition, Methodology, Resources, Writing – review and editing | Matthias Quick, Funding acquisition, Methodology, Resources, Writing – review and editing | Paul D. Roepe, Methodology, Project administration, Resources, Validation, Visualization, Writing – review and editing | Manuel Llinás, Conceptualization, Project administration, Resources, Writing – review and editing | David A. Fidock, Conceptualization, Data curation, Formal analysis, Investigation, Methodology, Validation, Writing – original draft, Writing – review and editing

ADDITIONAL FILES

The following material is available online.

Supplemental Material

Supplemental Material (mBio01832-23-s0001.pdf). Fig S1-S8 and Tables S1-S7.

REFERENCES

1. World Health Organization. 2022. World malaria report. Available from: https://www.who.int/teams/global-malaria-programme/reports/world-malaria-report-2022
2. White NJ, Pukrittayakamee S, Hien TT, Faiz MA, Mokuolu OA, Dondorp AM. 2014. Malaria. Lancet 383:723–735. https://doi.org/10.1016/S0140-6736(13)60024-0
3. Dhorda M, Amaratunga C, Dondorp AM. 2021. Artemisinin and multidrug-resistant *Plasmodium falciparum* - a threat for malaria control and elimination. Curr Opin Infect Dis 34:432–439. https://doi.org/10.1097/QCO.0000000000000766
4. Kakuru A, Natureeba P, Muhindo MK, Clark TD, Havlir DV, Cohan D, Dorsey G, Kamya MR, Ruel T. 2016. Malaria burden in a birth cohort of HIV-exposed uninfected ugandan infants living in a high malaria transmission setting. Malar J 15:500. https://doi.org/10.1186/s12936-016-1568-z
5. Gutman J, Kovacs S, Dorsey G, Stergachis A, Ter Kuile FO. 2017. Safety, tolerability, and efficacy of repeated doses of dihydroartemisinin-piperaquine for prevention and treatment of malaria: a systematic review and meta-analysis. Lancet Infect Dis 17:184–193. https://doi.org/10.1016/S1473-3099(16)30378-4
6. van der Pluijm RW, Tripura R, Hoglund RM, Pyae Phyo A, Lek D, ul Islam A, Anvikar AR, Satpathi P, Satpathi S, Behera PK, et al. 2020. Triple artemisinin-based combination therapies versus artemisinin-based combination therapies for uncomplicated *Plasmodium falciparum* malaria: a multicentre, open-label, randomised clinical trial. Lancet 395:1345–1360. https://doi.org/10.1016/S0140-6736(20)30552-3
7. Saunders DL, Vanachayangkul P, Lon C, U.S. Army Military Malaria Research Program National Center for Parasitology, Entomology, and Malaria Control (CNM); Royal Cambodian Armed Forces. 2014. Dihydroartemisinin-piperaquine failure in Cambodia. N Engl J Med 371:484–485. https://doi.org/10.1056/NEJMc1403007
8. Goldberg DE, Cowman AF. 2010. Moving in and renovating: exporting proteins from *Plasmodium* into host erythrocytes. Nat Rev Microbiol 8:617–621. https://doi.org/10.1038/nrmicro2420
9. Duru V, Khim N, Leang R, Kim S, Domergue A, Kloeung N, Ke S, Chy S, Eam R, Khean C, Loch K, Ken M, Lek D, Beghain J, Ariey F, Guerin PJ, Huy

R, Mercereau-Puijalon O, Witkowski B, Menard D. 2015. *Plasmodium falciparum* dihydroartemisinin-piperaquine failures in Cambodia are associated with mutant K13 parasites presenting high survival rates in novel piperaquine *in vitro* assays: retrospective and prospective investigations. BMC Med 13:305. https://doi.org/10.1186/s12916-015-0539-5

10. Dhingra SK, Redhi D, Combrinck JM, Yeo T, Okombo J, Henrich PP, Cowell AN, Gupta P, Stegman ML, Hoke JM, Cooper RA, Winzeler E, Mok S, Egan TJ, Fidock DA. 2017. A variant PfCRT isoform can contribute to *Plasmodium falciparum* resistance to the first-line partner drug piperaquine. mBio 8:e00303-17. https://doi.org/10.1128/mBio.00303-17
11. Agrawal S, Moser KA, Morton L, Cummings MP, Parihar A, Dwivedi A, Shetty AC, Drabek EF, Jacob CG, Henrich PP, Parobek CM, Jongsakul K, Huy R, Spring MD, Lanteri CA, Chaorattanakawee S, Lon C, Fukuda MM, Saunders DL, Fidock DA, Lin JT, Juliano JJ, Plowe CV, Silva JC, Takala-Harrison S. 2017. Association of a novel mutation in the *Plasmodium falciparum* chloroquine resistance transporter with decreased piperaquine sensitivity. J Infect Dis 216:468–476. https://doi.org/10.1093/infdis/jix334
12. Ross LS, Dhingra SK, Mok S, Yeo T, Wicht KJ, Kümpornsin K, Takala-Harrison S, Witkowski B, Fairhurst RM, Ariey F, Menard D, Fidock DA. 2018. Emerging Southeast Asian PfCRT mutations confer *Plasmodium falciparum* resistance to the first-line antimalarial piperaquine. Nat Commun 9:3314. https://doi.org/10.1038/s41467-018-05652-0
13. Hamilton WL, Amato R, van der Pluijm RW, Jacob CG, Quang HH, Thuy-Nhien NT, Hien TT, Hongvanthong B, Chindavongsa K, Mayxay M, et al. 2019. Evolution and expansion of multidrug-resistant malaria in Southeast Asia: a genomic epidemiology study. Lancet Infect Dis 19:943–951. https://doi.org/10.1016/S1473-3099(19)30392-5
14. van der Pluijm RW, Imwong M, Chau NH, Hoa NT, Thuy-Nhien NT, Thanh NV, Jittamala P, Hanboonkunupakarn B, Chutasmit K, Saelow C, et al. 2019. Determinants of dihydroartemisinin-piperaquine treatment failure in *Plasmodium falciparum* malaria in Cambodia, Thailand, and Vietnam: a prospective clinical, pharmacological, and genetic study. Lancet Infect Dis 19:952–961. https://doi.org/10.1016/S1473-3099(19)30391-3
15. Dhingra SK, Small-Saunders JL, Ménard D, Fidock DA. 2019. *Plasmodium falciparum* resistance to piperaquine driven by PfCRT. Lancet Infect Dis 19:1168–1169. https://doi.org/10.1016/S1473-3099(19)30543-2
16. Small-Saunders JL, Hagenah LM, Wicht KJ, Dhingra SK, Deni I, Kim J, Vendome J, Gil-Iturbe E, Roepe PD, Mehta M, Mancia F, Quick M, Eppstein MJ, Fidock DA. 2022. Evidence for the early emergence of piperaquine-resistant *Plasmodium falciparum* malaria and modeling strategies to mitigate resistance. PLoS Pathog 18:e1010278. https://doi.org/10.1371/journal.ppat.1010278
17. Kim J, Tan YZ, Wicht KJ, Erramilli SK, Dhingra SK, Okombo J, Vendome J, Hagenah LM, Giacometti SI, Warren AL, Nosol K, Roepe PD, Potter CS, Carragher B, Kossiakoff AA, Quick M, Fidock DA, Mancia F. 2019. Structure and drug resistance of the *Plasmodium falciparum* transporter PfCRT. Nature 576:315–320. https://doi.org/10.1038/s41586-019-1795-x
18. Riegel B, Roepe PD. 2020. Altered drug transport by *Plasmodium falciparum* chloroquine resistance transporter isoforms harboring mutations associated with piperaquine resistance. Biochemistry 59:2484–2493. https://doi.org/10.1021/acs.biochem.0c00247
19. Gomez GM, D'Arrigo G, Sanchez CP, Berger F, Wade RC, Lanzer M. 2023. PfCRT mutations conferring piperaquine resistance in falciparum malaria shape the kinetics of quinoline drug binding and transport. PLoS Pathog 19:e1011436. https://doi.org/10.1371/journal.ppat.1011436
20. Pulcini S, Staines HM, Lee AH, Shafik SH, Bouyer G, Moore CM, Daley DA, Hoke MJ, Altenhofen LM, Painter HJ, Mu J, Ferguson DJP, Llinás M, Martin RE, Fidock DA, Cooper RA, Krishna S. 2015. Mutations in the *Plasmodium falciparum* chloroquine resistance transporter, PfCRT, enlarge the parasite's food vacuole and alter drug sensitivities. Sci Rep 5:14552. https://doi.org/10.1038/srep14552
21. Okombo J, Mok S, Qahash T, Yeo T, Bath J, Orchard LM, Owens E, Koo I, Albert I, Llinás M, Fidock DA. 2022. Piperaquine-resistant PfCRT mutations differentially impact drug transport, hemoglobin catabolism and parasite physiology in *Plasmodium falciparum* asexual blood stages. PLoS Pathog 18:e1010926. https://doi.org/10.1371/journal.ppat.1010926
22. Gabryszewski SJ, Dhingra SK, Combrinck JM, Lewis IA, Callaghan PS, Hassett MR, Siriwardana A, Henrich PP, Lee AH, Gnädig NF, Musset L, Llinás M, Egan TJ, Roepe PD, Fidock DA. 2016. Evolution of fitness cost-neutral mutant PfCRT conferring *P. falciparum* 4-aminoquinoline drug resistance is accompanied by altered parasite metabolism and digestive vacuole physiology. PLoS Pathog 12:e1005976. https://doi.org/10.1371/journal.ppat.1005976
23. Bopp S, Magistrado P, Wong W, Schaffner SF, Mukherjee A, Lim P, Dhorda M, Amaratunga C, Woodrow CJ, Ashley EA, White NJ, Dondorp AM, Fairhurst RM, Ariey F, Menard D, Wirth DF, Volkman SK. 2018. Plasmepsin II-III copy number accounts for bimodal piperaquine resistance among Cambodian *Plasmodium falciparum*. Nat Commun 9:1769. https://doi.org/10.1038/s41467-018-04104-z
24. Gabryszewski SJ, Modchang C, Musset L, Chookajorn T, Fidock DA. 2016. Combinatorial genetic modeling of PfCRT-mediated drug resistance evolution in *Plasmodium falciparum*. Mol Biol Evol 33:1554–1570. https://doi.org/10.1093/molbev/msw037
25. Petersen I, Gabryszewski SJ, Johnston GL, Dhingra SK, Ecker A, Lewis RE, de Almeida MJ, Straimer J, Henrich PP, Palatulan E, Johnson DJ, Coburn-Flynn O, Sanchez C, Lehane AM, Lanzer M, Fidock DA. 2015. Balancing drug resistance and growth rates via compensatory mutations in the *Plasmodium falciparum* chloroquine resistance transporter. Mol Microbiol 97:381–395. https://doi.org/10.1111/mmi.13035
26. Imwong M, Suwannasin K, Srisutham S, Vongpromek R, Promnarate C, Saejeng A, Phyo AP, Proux S, Pongvongsa T, Chea N, et al. 2021. Evolution of multidrug resistance in *Plasmodium falciparum*: a longitudinal study of genetic resistance markers in the Greater Mekong Subregion. Antimicrob Agents Chemother 65:e0112121. https://doi.org/10.1128/AAC.01121-21
27. MalariaGEN, Abdel Hamid MM, Abdelraheem MH, Acheampong DO, Ahouidi A, Ali M, Almagro-Garcia J, Amambua-Ngwa A, Amaratunga C, Amenga-Etego L, Andagalu B, Anderson T, Andrianaranjaka V, Aniebo I, Aninagyei E, Ansah F, Ansah PO, Apinjoh T, Arnaldo P, Ashley E, Auburn S, Awandare GA, Ba H, Baraka V, Barry A, et al. 2023. Pf7: an open dataset of *Plasmodium falciparum* genome variation in 20,000 worldwide samples. Wellcome Open Res 8:22. https://doi.org/10.12688/wellcomeopenres.18681.1
28. Straimer J, Lee MCS, Lee AH, Zeitler B, Williams AE, Pearl JR, Zhang L, Rebar EJ, Gregory PD, Llinás M, Urnov FD, Fidock DA. 2012. Site-specific genome editing in *Plasmodium falciparum* using engineered zinc-finger nucleases. Nat Methods 9:993–998. https://doi.org/10.1038/nmeth.2143
29. Dhingra SK, Gabryszewski SJ, Small-Saunders JL, Yeo T, Henrich PP, Mok S, Fidock DA, Miller LH. 2019. Global spread of mutant PfCRT and its pleiotropic impact on *Plasmodium falciparum* multidrug resistance and fitness. mBio 10:e02731-18. https://doi.org/10.1128/mBio.02731-18
30. Witkowski B, Duru V, Khim N, Ross LS, Saintpierre B, Beghain J, Chy S, Kim S, Ke S, Kloeung N, et al. 2017. A surrogate marker of piperaquine-resistant *Plasmodium falciparum* malaria: a phenotype-genotype association study. Lancet Infect Dis 17:174–183. https://doi.org/10.1016/S1473-3099(16)30415-7
31. Callaghan PS, Hassett MR, Roepe PD. 2015. Functional comparison of 45 naturally occurring isoforms of the *Plasmodium falciparum* chloroquine resistance transporter (PfCRT). Biochemistry 54:5083–5094. https://doi.org/10.1021/acs.biochem.5b00412
32. Willems A, Kalaw A, Ecer A, Kotwal A, Roepe LD, Roepe PD. 2023. Structures of *Plasmodium falciparum* chloroquine resistance transporter (PfCRT) isoforms and their interactions with chloroquine. Biochemistry 62:1093–1110. https://doi.org/10.1021/acs.biochem.2c00669
33. Sanchez CP, Manson EDT, Moliner Cubel S, Mandel L, Weidt SK, Barrett MP, Lanzer M. 2022. The knock-down of the chloroquine resistance transporter PfCRT is linked to oligopeptide handling in *Plasmodium falciparum*. Microbiol Spectr 10:e0110122. https://doi.org/10.1128/spectrum.01101-22
34. Shafik SH, Cobbold SA, Barkat K, Richards SN, Lancaster NS, Llinás M, Hogg SJ, Summers RL, McConville MJ, Martin RE. 2020. The natural function of the malaria parasite's chloroquine resistance transporter. Nat Commun 11:3922. https://doi.org/10.1038/s41467-020-17781-6
35. Amato R, Lim P, Miotto O, Amaratunga C, Dek D, Pearson RD, Almagro-Garcia J, Neal AT, Sreng S, Suon S, Drury E, Jyothi D, Stalker J, Kwiatkowski DP, Fairhurst RM. 2017. Genetic markers associated with dihydroartemisinin-piperaquine failure in *Plasmodium falciparum* malaria in Cambodia: a genotype-phenotype association study. Lancet Infect Dis 17:164–173. https://doi.org/10.1016/S1473-3099(16)30409-1
36. Frosch AEP, Laufer MK, Mathanga DP, Takala-Harrison S, Skarbinski J, Claassen CW, Dzinjalamala FK, Plowe CV. 2014. Return of widespread

chloroquine-sensitive *Plasmodium falciparum* to Malawi. J Infect Dis 210:1110–1114. https://doi.org/10.1093/infdis/jiu216
37. Takala-Harrison S, Laufer MK. 2015. Antimalarial drug resistance in Africa: key lessons for the future. Ann N Y Acad Sci 1342:62–67. https://doi.org/10.1111/nyas.12766
38. Wicht KJ, Small-Saunders JL, Hagenah LM, Mok S, Fidock DA. 2022. Mutant PfCRT can mediate piperaquine resistance in African *Plasmodium falciparum* with reduced fitness and increased susceptibility to other antimalarials. J Infect Dis 226:2021–2029. https://doi.org/10.1093/infdis/jiac365
39. Martin RE, Marchetti RV, Cowan AI, Howitt SM, Bröer S, Kirk K. 2009. Chloroquine transport via the malaria parasite's chloroquine resistance transporter. Science 325:1680–1682. https://doi.org/10.1126/science.1175667
40. Kuhn Y, Rohrbach P, Lanzer M. 2007. Quantitative pH measurements in *Plasmodium falciparum*-infected erythrocytes using pHluorin. Cell Microbiol 9:1004–1013. https://doi.org/10.1111/j.1462-5822.2006.00847.x
41. Kirk K, Lehane AM. 2014. Membrane transport in the malaria parasite and its host erythrocyte. Biochem J 457:1–18. https://doi.org/10.1042/BJ20131007
42. Krugliak M, Zhang J, Ginsburg H. 2002. Intraerythrocytic *Plasmodium falciparum* utilizes only a fraction of the amino acids derived from the digestion of host cell cytosol for the biosynthesis of its proteins. Mol Biochem Parasitol 119:249–256. https://doi.org/10.1016/s0166-6851(01)00427-3
43. Lee AH, Dhingra SK, Lewis IA, Singh MK, Siriwardana A, Dalal S, Rubiano K, Klein MS, Baska KS, Krishna S, Klemba M, Roepe PD, Llinás M, Garcia CRS, Fidock DA. 2018. Evidence for regulation of hemoglobin metabolism and intracellular ionic flux by the *Plasmodium falciparum* chloroquine resistance transporter. Sci Rep 8:13578. https://doi.org/10.1038/s41598-018-31715-9
44. Boni MF, Smith DL, Laxminarayan R. 2008. Benefits of using multiple first-line therapies against malaria. Proc Natl Acad Sci U S A 105:14216–14221. https://doi.org/10.1073/pnas.0804628105
45. Smith DL, Klein EY, McKenzie FE, Laxminarayan R. 2010. Prospective strategies to delay the evolution of anti-malarial drug resistance: weighing the uncertainty. Malar J 9:217. https://doi.org/10.1186/1475-2875-9-217
46. Boni MF, White NJ, Baird JK. 2016. The community as the patient in malaria-endemic areas: preempting drug resistance with multiple first-line therapies. PLoS Med 13:e1001984. https://doi.org/10.1371/journal.pmed.1001984
47. Zupko RJ, Nguyen TD, Somé AF, Tran T-A, Gerardin J, Dudas P, Giang DDH, Tran KT, Wesolowski A, Ouédraogo J-B, Boni MF. 2022. Long-term effects of increased adoption of artemisinin combination therapies in Burkina Faso. PLOS Glob Public Health 2:e0000111. https://doi.org/10.1371/journal.pgph.0000111
48. Deni I, Stokes BH, Ward KE, Fairhurst KJ, Pasaje CFA, Yeo T, Akbar S, Park H, Muir R, Bick DS, et al. 2023. Mitigating the risk of antimalarial resistance via covalent dual-subunit inhibition of the *Plasmodium p*roteasome. Cell Chem Biol 30:470–485. https://doi.org/10.1016/j.chembiol.2023.03.002
49. Fidock DA, Nomura T, Wellems TE. 1998. Cycloguanil and its parent compound proguanil demonstrate distinct activities against *Plasmodium falciparum* malaria parasites transformed with human dihydrofolate reductase. Mol Pharmacol 54:1140–1147. https://doi.org/10.1124/mol.54.6.1140
50. Stokes BH, Dhingra SK, Rubiano K, Mok S, Straimer J, Gnädig NF, Deni I, Schindler KA, Bath JR, Ward KE, et al. 2021. *Plasmodium falciparum* K13 mutations in Africa and Asia impact artemisinin resistance and parasite fitness. Elife 10:e66277. https://doi.org/10.7554/eLife.66277
51. Goehring A, Lee CH, Wang KH, Michel JC, Claxton DP, Baconguis I, Althoff T, Fischer S, Garcia KC, Gouaux E. 2014. Screening and large-scale expression of membrane proteins in mammalian cells for structural studies. Nat Protoc 9:2574–2585. https://doi.org/10.1038/nprot.2014.173
52. Wright DJ, O'Reilly M, Tisi D. 2018. Engineering and purification of a thermostable, high-yield, variant of PfCRT, the *Plasmodium falciparum* chloroquine resistance transporter. Protein Expr Purif 141:7–18. https://doi.org/10.1016/j.pep.2017.08.005
53. Kozlowski LP. 2021. IPC 2.0: prediction of isoelectric point and pKa dissociation constants. Nucleic Acids Res 49:W285–W292. https://doi.org/10.1093/nar/gkab295
54. Bowers KJ, Sacerdoti FD, Salmon JK, Shan Y, Shaw DE, Chow E, Xu H, Dror RO, Eastwood MP, Gregersen BA, Klepeis JL, Kolossvary I, Moraes MA, SacerdotiFD, SalmonJK, ShanY, Shaw DE. 2006. Molecular dynamics - scalable algorithms for molecular dynamics simulations on commodity clusters. In Proceedings of the ACM/IEEE SC2006 Conference on High Performance Networking and Computing. Tampa, FL, USA.
55. Sastry GM, Adzhigirey M, Day T, Annabhimoju R, Sherman W. 2013. Protein and ligand preparation: parameters, protocols, and influence on virtual screening enrichments. J Comput Aided Mol Des 27:221–234. https://doi.org/10.1007/s10822-013-9644-8
56. Jacobson MP, Pincus DL, Rapp CS, Day TJF, Honig B, Shaw DE, Friesner RA. 2004. A hierarchical approach to all-atom protein loop prediction. Proteins 55:351–367. https://doi.org/10.1002/prot.10613
57. Frey BJ, Dueck D. 2007. Clustering by passing messages between data points. Science 315:972–976. https://doi.org/10.1126/science.1136800
58. Shivender Shandilya JV. 2016. Thomas holder colorByRMSD. Available from: https://raw.githubusercontent.com/Pymol-Scripts/Pymol-script1025 repo/master/colorbyrmsd.py
59. Humphrey W, Dalke A, Schulten K. 1996. VMD: visual molecular dynamics. J Mol Graph 14:33–38. https://doi.org/10.1016/0263-7855(96)00018-5

Supplemental Material

Additional PfCRT Mutations Driven By Selective Pressure for Improved Fitness Can Result in the Loss of Piperaquine Resistance and Altered *Plasmodium falciparum* Physiology

Laura M. Hagenah, Satish K. Dhingra, Jennifer L. Small-Saunders, Tarrick Qahash, Andreas Willems, Kyra A. Schindler, Gabriel W. Rangel, Eva Gil-Iturbe, Jonathan Kim, Emiliya Akhundova, Tomas Yeo, John Okombo, Filippo Mancia, Matthias Quick, Paul D. Roepe, Manuel Llinás, David A. Fidock

Supplemental Figures and Tables

Figure S1: Zinc-finger nuclease (ZFN)-mediated editing of *pfcrt*……page 2
Figure S2: Cell morphology of *pfcrt*-edited parasites ……..page 3
Figure S3: IC_{50} values for relevant antimalarials…….……..page 4
Figure S4: Mapping of mutations onto the PfCRT structure.....……page 5
Figure S5: Visual representation of salt bridge interactions broken as Dd2 PfCRT evolves to any of the F145I mutant isoforms……...page 6
Figure S6: Venn diagram of numbers of significantly altered peptides …….....page 7
Figure S7: Number of differentially accumulated peptides shown as a function of peptide charge of accumulated peptides at pH 5.5 or 7.4 …….....page 8
Figure S8: Peptides HVDDM and VDPVNF inhibit ^{3}H-PPQ and ^{3}H-CQ transport via PfCRT…….page 9
Table S1: Piperaquine survival assay (PSA) values of *pfcrt*-modified parasite lines……page 10
Table S2: Mean IC_{50} and IC_{90} values of *pfcrt*-modified parasite lines…….....page 11
Table S3: Transport in proteoliposomes……..…….....page 12
Table S4: All salt bridges found for all PfCRT isoforms……..……..……..……..……page 13
Table S5: Averaged $\log_2$ fold change of the baseline peptide levels in the variant PfCRT lines versus $Dd2^{Dd2+F145I}$…….....page 14
Table S6: List of peptides showing significantly different levels in $Dd2^{Dd2}$, $Dd2^{Dd2+F145I+F131C}$, $Dd2^{Dd2+F145I+I347T}$, and $Dd2^{Dd2+F145I+C258W}$ compared to $Dd2^{Dd2+F145I}$……..page 16
Table S7: List of oligonucleotides used in this study……page 18

SUPPLEMENTAL REFERENCES……page 19

Figure S1

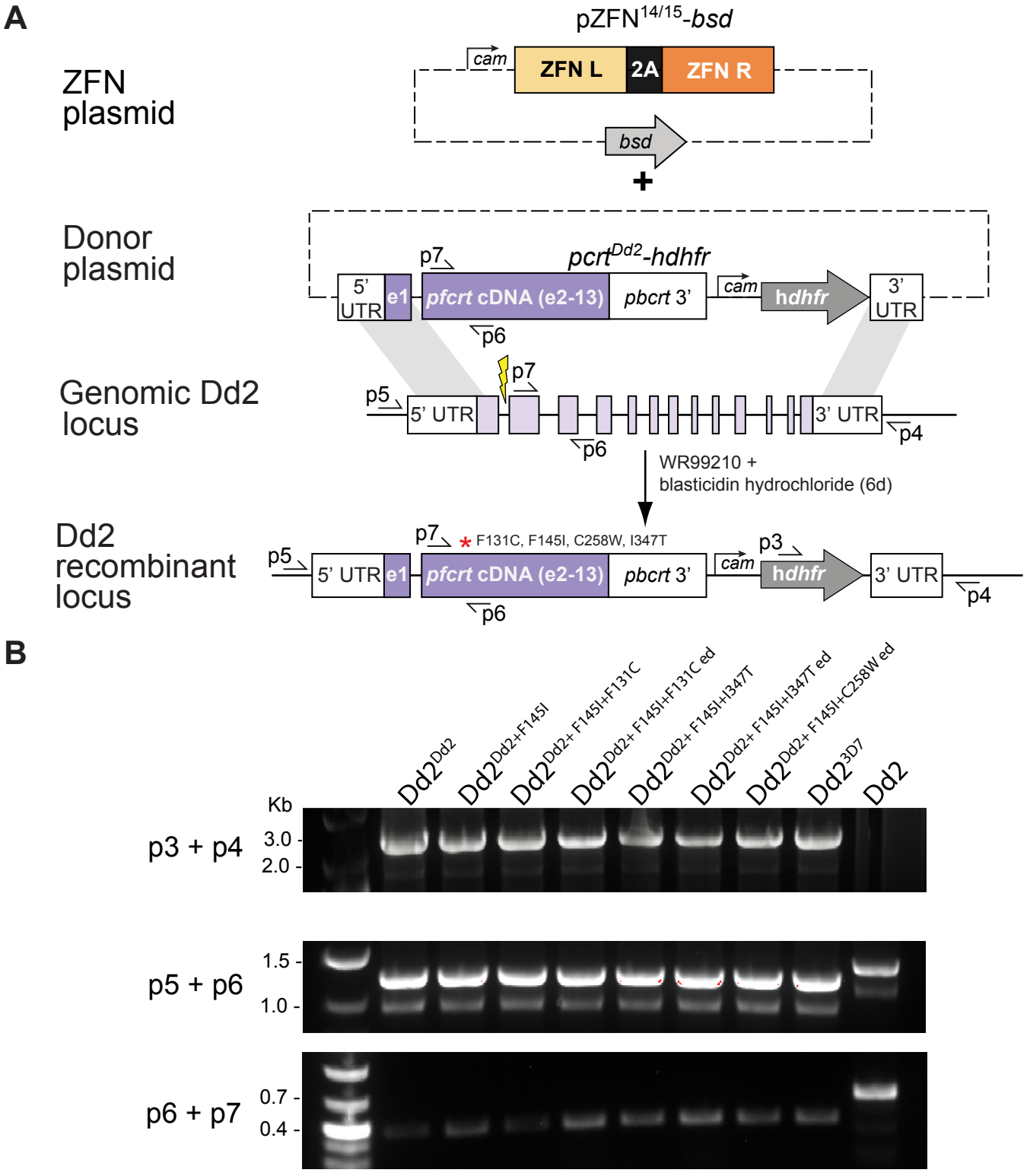

Fig. S1. Zinc-finger nuclease (ZFN)-mediated editing of *pfcrt*. (**A**) The *pfcrt* gene was edited using a two-plasmid approach, one containing the homologous donor template and the other containing the *pfcrt*-specific pair of ZFNs linked by a 2A ribosome skip peptide (1). Parasites were selected for the human dihydrofolate reductase (h*dhfr*) and the blasticidin S-deaminase (BSD) markers with WR99210 and blasticidin hydrochloride, respectively. (**B**) Three sets of PCRs were performed to confirm editing and the modified locus was verified by Sanger sequencing. Primer locations are denoted in (**A**), and sequences are listed in **Table S7**.

Figure S2

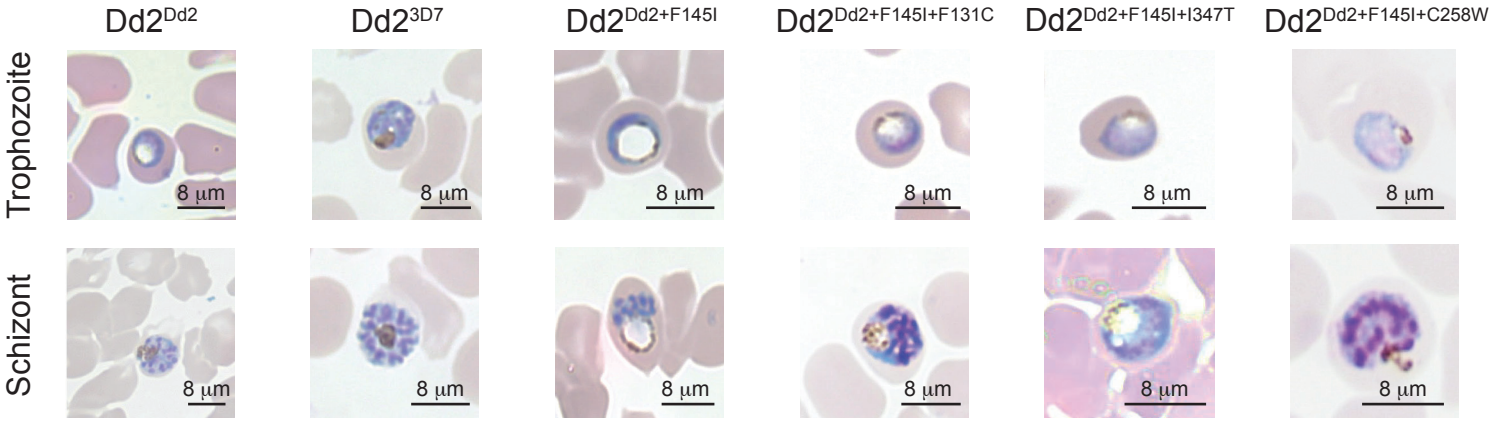

Fig. S2. Cell morphology of *pfcrt*-edited parasites. Dd2$^{Dd2+F145I}$ has distended digestive vacuoles characteristic of piperaquine-resistant parasites in both the trophozoite and schizont asexual blood stages. Dd2$^{Dd2+F145I+F131C}$, Dd2$^{Dd2+F145I+I347T}$, and Dd2$^{Dd2+F145I+C258W}$ vacuoles appear smaller compared to Dd2$^{Dd2+F145I}$. Note that the partially bloated vacuoles evident in Dd2$^{Dd2+F145I+F131C}$ and Dd2$^{Dd2+F145I+I347T}$ associate with a minimal change in peptide accumulation relative to Dd2$^{Dd2+F145I}$ (**Fig. 4**).

Figure S3

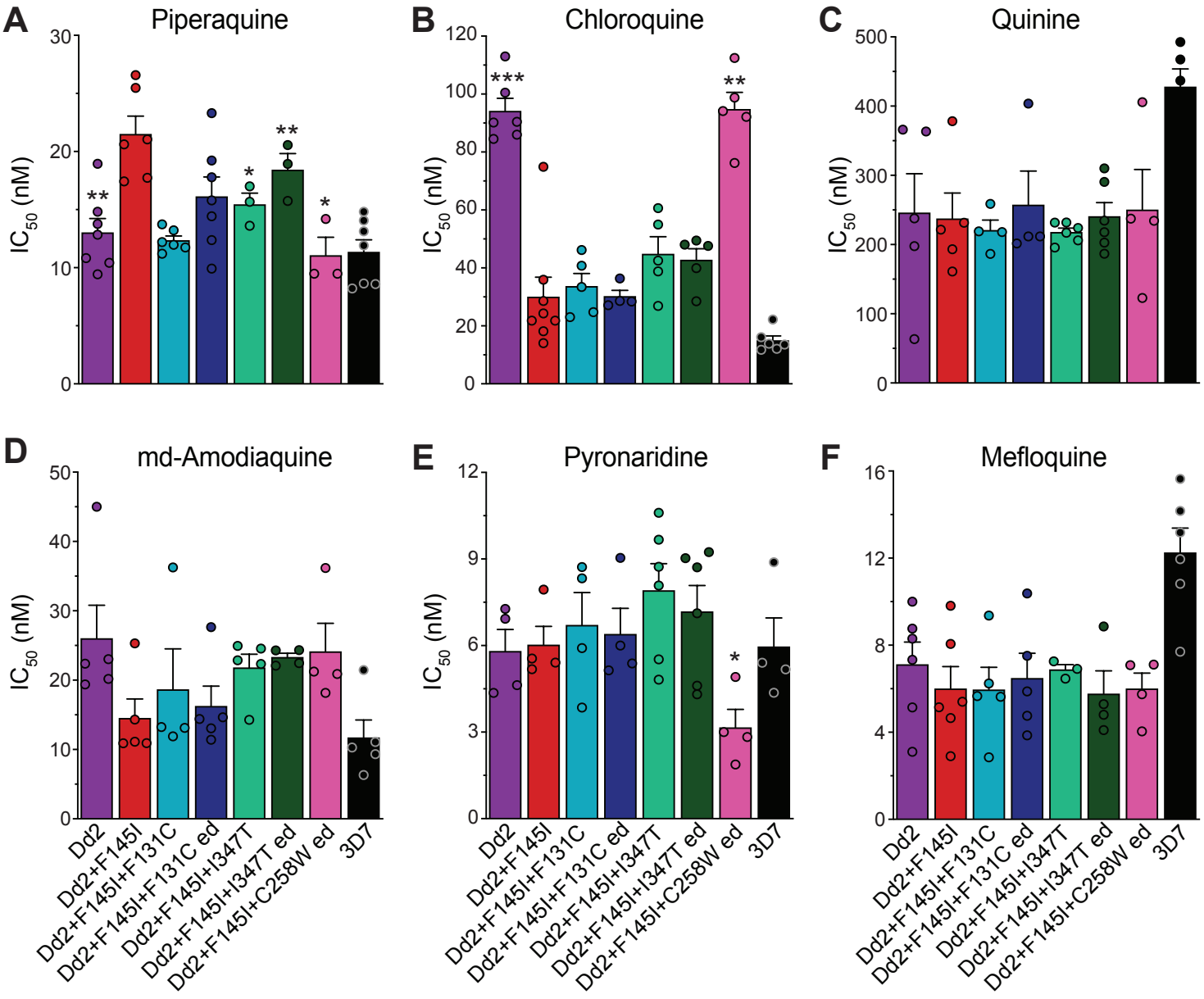

Fig. S3. IC_{50} values for relevant antimalarials. Mean ± SEM IC_{50} values (**Table S2**) were calculated from 72-hr dose-response assays for: (**A**) Piperaquine; (**B**) Chloroquine; (**C**) Quinine; (**D**) monodesethyl (md)-Amodiaquine; (**E**) Pyronaridine; and (**F**) Mefloquine. N, n = 4-7, 2. Statistical significance was determined using Mann-Whitney *U* tests as compared to the isogenic $Dd2^{Dd2+F145I}$ line. **P* < 0.05; ***P* < 0.01; ****P* < 0.001. Individual circles indicate values from each independent experiment.

Figure S4

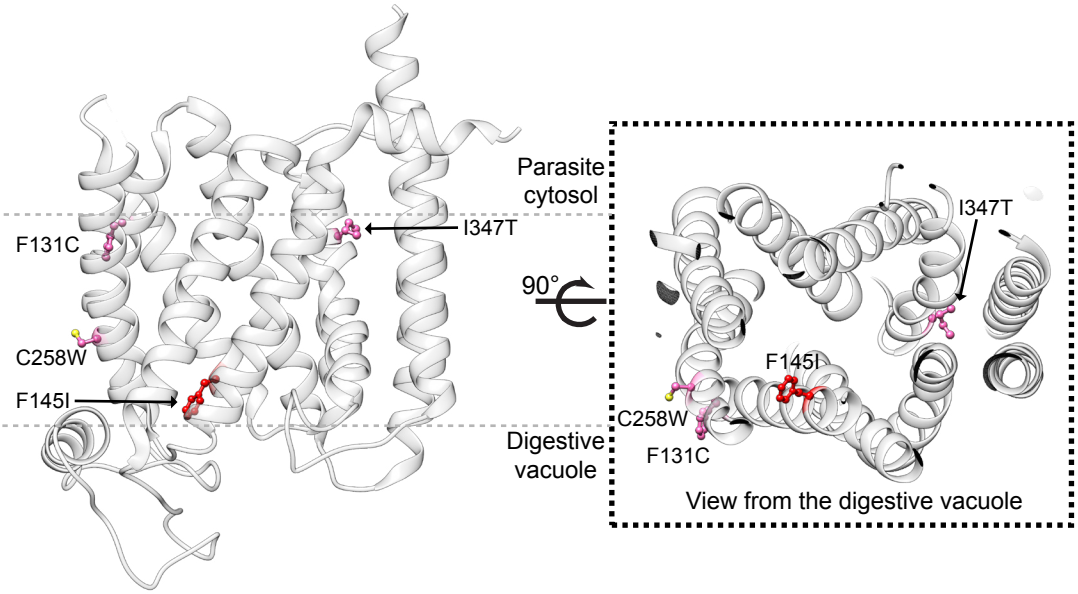

Fig. S4. Mapping of mutations onto the PfCRT structure. F145I, F131C, C258W, and I347T are mapped onto the known 7G8 cryo-EM structure (2). Mutations have their side chains rendered as sticks and are colored in red (F145I) or pink (F131C, C258W and I347T). The remaining structures are rendered in cartoon and colored in white. Views are shown vertically (digestive vacuole to the bottom) and rotated to show the structure from the digestive vacuole side.

Figure S5

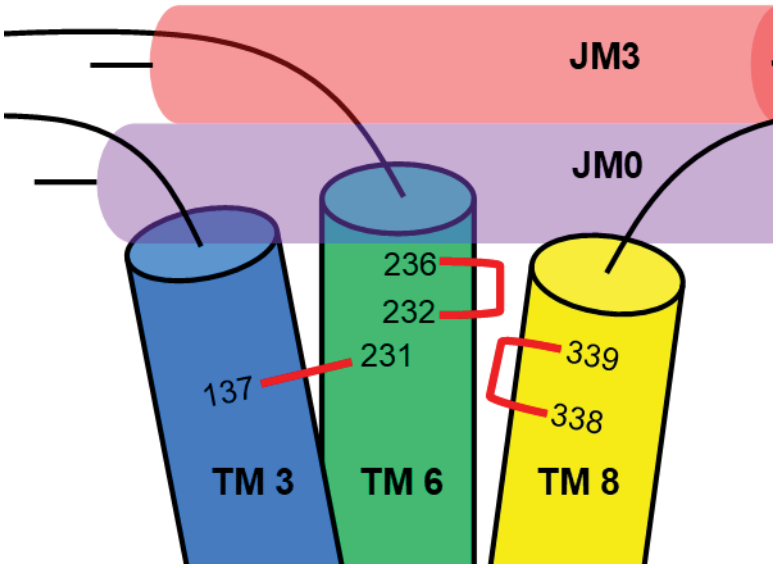

Fig. S5. Visual representation of salt bridge interactions broken as Dd2 PfCRT evolves to any of the F145I mutant isoforms. Transmembrane (TM) helix numbers are denoted, with PfCRT "zipper" bundled helices JM3 and JM0 shown above [3]. The full list off salt bridge interactions is listed in **Table S4**.

Figure S6

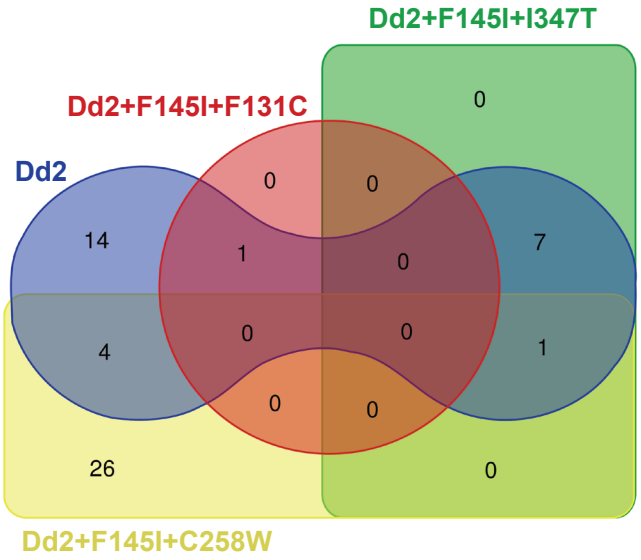

Fig. S6. Venn diagram of numbers of significantly altered peptides. Venn diagram showing numbers of peptides whose levels were significantly increased or decreased peptides for the lines $Dd2^{Dd2}$ (blue), $Dd2^{Dd2+F145I+F131C}$ (red), $Dd2^{Dd2+F145I+I347T}$ (green), or $Dd2^{Dd2+F145I+C258W}$ (yellow), relative to the isogenic $Dd2^{Dd2+F145I}$ line. The largest numbers of differences were observed with $Dd2^{Dd2+F145I+C258W}$ and $Dd2^{Dd2}$, as reflected in the heatmap (**Fig. 4A**) that showed these two lines being the most divergent compared with $Dd2^{Dd2+F145I}$. Significance was attributed to a peptide when it showed a statistically significant difference ($P < 0.05$) between the $Dd2^{Dd2+F145I}$ reference line and an isogenic test line (Student's *t* test, data obtained from 3 independent experiments; see **Table S6**).

Figure S7

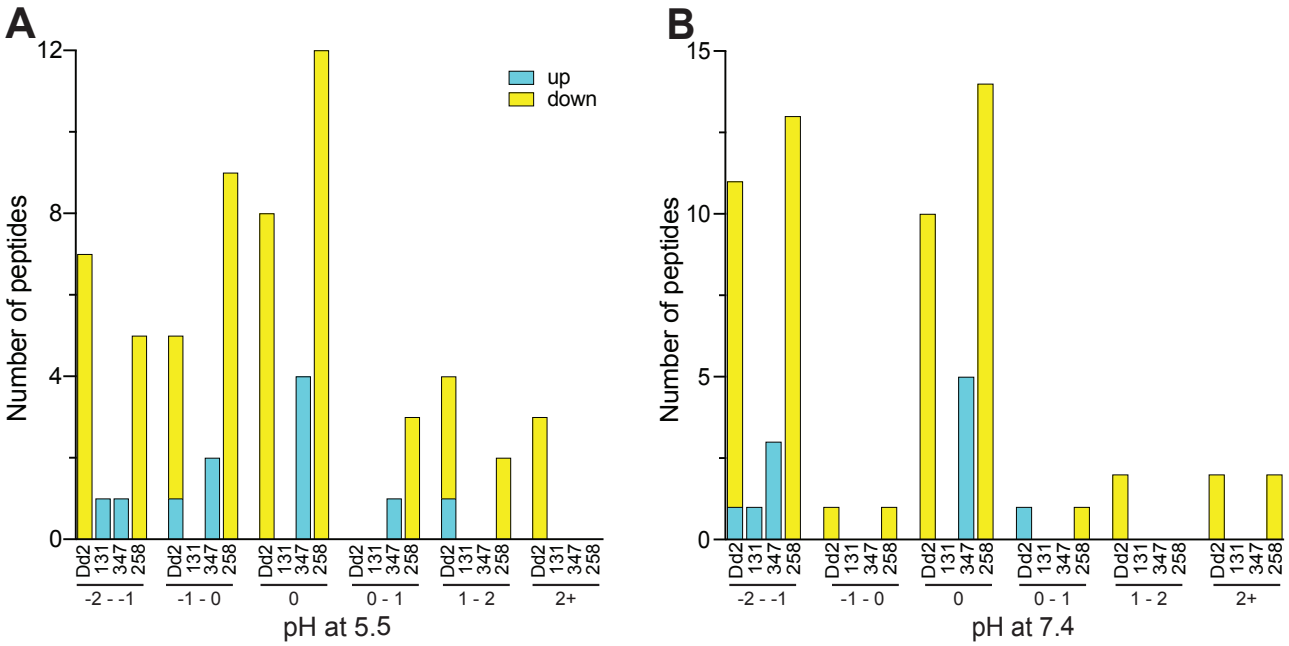

Fig. S7. Number of differentially accumulated peptides shown as a function of peptide charge of accumulated peptides at pH 5.5 or 7.4. Plots show differences in peptide levels between lines with a given mutation and Dd2$^{Dd2+F145I}$. Peptides are classified by (**A**) charge at pH 5.5 (representing the DV lumen) or (**B**) charge at pH 7.4 (representing the cytosol). Details are provided in **Table S6**.

Figure S8

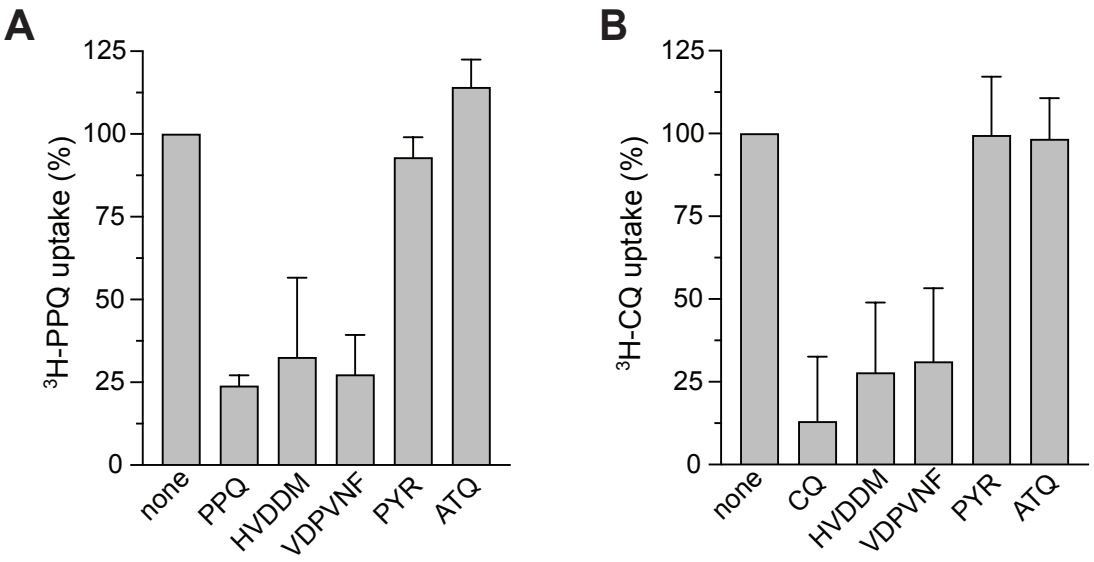

Fig. S8. Peptides HVDDM and VDPVNF inhibit ^{3}H-PPQ and ^{3}H-CQ transport via PfCRT. Uptake of (**A**) 50 nM ^{3}H-PPQ by 7G8+F145I PfCRT or (**B**) ^{3}H-CQ by 7G8 PfCRT was measured for 1 min in the presence or absence of the 25 μM HVDDM or VDPVNF. Values were normalized to the signal in the absence of the non-radiolabelled compound (”none”). CQ, PPQ, and the non-PfCRT related drugs pyrimethamine (PYR) and atovaquone (ATQ) were also tested at 25 μM. Data are means ± s.d. of 3 independent experiments.

Table S1 Piperaquine survival assay values of *pfcrt*-modified parasite lines.

	$Dd2^{Dd2}$	$Dd2^{3D7}$	$Dd2^{Dd2+F145I}$	$Dd2^{Dd2+F145I+F131C}$	$Dd2^{Dd2+F145I+F131C}$ (edited)	$Dd2^{Dd2+F145I+I347T}$	$Dd2^{Dd2+F145I+I347T}$ (edited)	$Dd2^{Dd2+F145I+C258W}$ (edited)
1600 nM	**3.5 ± 0.7**	**2.9 ± 1.5**	**35.0 ± 2.0**	**28.4 ± 3.6**	**33.6 ± 1.0**	**6.7 ± 1.1**	**13.3 ± 1.9**	**3.2 ± 0.6**
N	4	6	7	7	8	3	2	3
P vs $Dd2^{Dd2}$	–	0.61	0.006	0.006	0.010	0.11	0.13	>0.99
P vs $Dd2^{Dd2+F145I}$	0.006	–	–	0.24	0.51	0.056	0.017	0.017
800 nM	**3.1 ± 1.1**	**3.3 ± 0.5**	**32.9 ± 3.0**	**28.5 ± 2.9**	**30.5 ± 2.0**	**2.9 ± 1.5**	**5.9 ± 4.5**	**3.3 ± 0.7**
N	4	6	7	7	7	3	2	3
P vs $Dd2^{Dd2}$	–	>0.99	0.006	0.006	0.006	0.86	0.80	0.86
P vs $Dd2^{Dd2+F145I}$	0.006	–	–	0.30	0.59	0.017	0.056	0.017
400 nM	**3.3 ± 0.8**	**2.5 ± 0.5**	**23.1 ± 2.4**	**18.8 ± 3.2**	**19.2 ± 2.3**	**1.9 ± 0.3**	**2.9 ± 0.6**	**3.3 ± 0.7**
N	4	6	7	7	8	3	2	3
P vs $Dd2^{Dd2}$	–	0.35	0.010	0.010	0.006	0.40	0.80	>0.99
P vs $Dd2^{Dd2+F145I}$	0.010	–	–	0.12	0.22	0.024	0.071	0.024
200 nM	**3.8 ± 0.8**	**2.8 ± 0.6**	**18.4 ± 3.4**	**14.2 ± 2.4**	**12.1 ± 1.7**	**1.7 ± 0.2**	**3.2 ± 0.7**	**4.3 ± 1.1**
N	4	6	6	7	8	3	2	3
P vs $Dd2^{Dd2}$	–	0.26	0.010	0.006	0.016	0.40	0.53	>0.99
P vs $Dd2^{Dd2+F145I}$	0.010	–	–	0.17	0.23	0.024	0.071	0.024
100 nM	**4.3 ± 0.9**	**2.8 ± 0.5**	**15.4 ± 2.4**	**14.2 ± 2.4**	**10.1 ± 1.3**	**1.4 ± 0.1**	**4.2 ± 0.9**	**4.5 ± 1.1**
N	4	6	6	8	8	3	2	3
P vs $Dd2^{Dd2}$	–	0.26	0.010	0.004	0.038	0.057	0.53	>0.99
P vs $Dd2^{Dd2+F145I}$	0.010	–	–	0.47	0.12	0.024	0.071	0.024
50 nM	**4.1 ± 0.06**	**2.4 ± 0.5**	**17.5 ± 2.6**	**18.6 ± 2.9**	**11.9 ± 3.0**	**1.6 ± 0.4**	**2.6 ± 0.7**	**26.3 ± 13.7**
N	4	6	7	7	8	3	2	3
P vs $Dd2^{Dd2}$	–	0.038	0.005	0.010	0.010	0.057	0.13	0.057
P vs $Dd2^{Dd2+F145I}$	0.005	–	–	0.78	0.17	0.024	0.071	>0.99
25 nM	**8.5 ± 1.5**	**5.0 ± 1.0**	**18.2 ± 4.3**	**28.8 ± 5.9**	**36.1 ± 7.2**	**22.2 ± 6.1**	**20.4 ± 11.4**	**50.8 ± 18.3**
N	5	6	5	6	8	3	2	3
P vs $Dd2^{Dd2}$	–	0.13	0.016	0.009	0.008	0.38	0.14	0.036
P vs $Dd2^{Dd2+F145I}$	0.016	–	–	0.40	0.048	0.96	0.81	0.054
12.5 nM	**28.8 ± 5.3**	**44.7 ± 1.1**	**53.8 ± 5.4**	**38.6 ± 7.1**	**67.1 ± 7.7**	**58.6 ± 9.8**	**58.0 ± 24.7**	**75.9 ± 15.8**
N	4	6	7	6	4	3	2	3
P vs $Dd2^{Dd2}$	–	0.016	0.006	0.35	0.029	0.057	0.53	0.057
P vs $Dd2^{Dd2+F145I}$	0.006	–	–	0.35	0.15	0.95	>0.99	0.25
6.25 nM	**58.6 ± 6.5**	**77.6 ± 3.0**	**69.2 ± 3.2**	**54.2 ± 6.3**	**79.2 ± 5.1**	**78.3 ± 4.4**	**70.6 ± 5.1**	**89.0 ± 4.0**
N	4	5	7	6	8	3	2	3
P vs $Dd2^{Dd2}$	–	0.032	0.21	0.91	0.064	0.057	>0.99	0.057
P vs $Dd2^{Dd2+F145I}$	0.21	–	–	0.093	0.10	0.17	>0.99	0.033
3.125 nM	**79.0 ± 3.0**	**89.9 ± 2.2**	**82.9 ± 2.9**	**69.7 ± 5.1**	**87.4 ± 3.0**	**92.6 ± 12.4**	**99.6 ± 0.0**	**91.5 ± 3.1**
N	4	4	7	5	5	2	1	3
P vs $Dd2^{Dd2}$	–	0.057	0.39	0.11	0.19	0.53	–	0.11
P vs $Dd2^{Dd2+F145I}$	0.39	–	–	0.043	0.25	0.47	–	0.18

Piperaquine survival assay (PSA) values (nM) indicate the mean ± SEM, as determined in 2 to 8 independent assays performed in duplicate. Parasite survival is defined as the ratio of the parasitemias of the PPQ-treated to the no-drug control wells. This assay measures the survival of synchronous ring-stage parasites (0-6 hr post-invasion) exposed to PPQ for 72 hr, prior to measuring parasitemias by flow cytometry. N, number of independent assays. Statistical significance was determined via non-parametric Mann-Whitney *U* tests. *P* values are reported for comparisons with the parasite lines $Dd2^{Dd2}$ and $Dd2^{Dd2+F145I}$.

*$P < 0.05$ **$P < 0.01$

Table S2 Mean IC_{50} and IC_{90} values of *pfcrt*-modified parasite lines.

	$Dd2^{Dd2}$	$Dd2^{3D7}$	$Dd2^{Dd2+F145I}$	$Dd2^{Dd2+F145I+F131C}$	$Dd2^{Dd2+F145I+F131C}$ (edited)	$Dd2^{Dd2+F145I+I347T}$	$Dd2^{Dd2+F145I+I347T}$ (edited)	$Dd2^{Dd2+F145I+C258W}$ (edited)
PPQ IC_{50} (nM)	**13.0 ± 1.3**	**11.4 ± 1.1**	**21.5 ± 1.6**	**12.3 ± 0.4**	**16.1 ± 1.7**	**15.4 ± 1.0**	**18.4 ± 1.4**	**11.1 ± 1.5**
N	7	7	6	6	7	3	3	3
P vs $Dd2^{Dd2}$	–	0.40	0.005	0.21	0.95	0.27	0.007	0.48
P vs $Dd2^{Dd2+F145I}$	0.005	–	–	0.002	0.073	0.024	0.26	0.024
PPQ IC_{90} (nM)	**23.7 ± 1.9**	**23.6 ± 3.5**	**5636 ± 690.9**	**3601 ± 236.6**	**2753 ± 225.9**	**28.1 ± 4.2**	**30.1 ± 3.3**	**22.6 ± 2.0**
P vs $Dd2^{Dd2}$	–	0.96	0.006	0.017	0.017	0.27	0.022	>0.99
P vs $Dd2^{Dd2+F145I}$	0.006	0.004	–	0.057	0.057	0.016	0.010	0.032
CQ IC_{50} (nM)	**94.1 ± 4.4**	**14.9 ± 1.6**	**30.0 ± 6.9**	**33.6 ± 4.5**	**30.1 ± 2.1**	**44.8 ± 6.0**	**42.7 ± 3.9**	**94.7 ± 5.8**
N	6	6	8	5	4	5	5	5
P vs $Dd2^{Dd2}$	–	0.002	0.001	0.004	0.010	0.004	0.004	0.792
P vs $Dd2^{Dd2+F145I}$	0.001	–	–	0.208	0.301	0.061	0.061	0.002
CQ IC_{90} (nM)	**172.2 ± 18.5**	**21.9 ± 3.0**	**63.1 ± 20.1**	**60.2 ± 10.4**	**65.4 ± 6.7**	**98.7 ± 8.7**	**103.7 ± 5.7**	**175.1 ± 22.7**
P vs $Dd2^{Dd2}$	–	0.002	0.015	0.002	0.010	0.015	0.002	0.75
P vs $Dd2^{Dd2+F145I}$	0.015	–	–	0.31	0.41	0.15	0.15	0.032
md-CQ IC_{50} (nM)	**572.7 ± 77.6**	**21.1 ± 2.8**	**124.6 ± 19.6**	**165.7 ± 17.0**	**180.8 ± 20.6**	**205.8 ± 39.9**	**192.4 ± 26.8**	**840.8 ± 95.7**
N	6	6	5	5	4	5	5	4
P vs $Dd2^{Dd2}$	–	0.002	0.004	0.004	0.004	0.004	0.004	0.083
P vs $Dd2^{Dd2+F145I}$	0.004	–	–	0.31	0.095	0.095	0.032	0.008
md-CQ IC_{90} (nM)	**1152 ± 143.2**	**347.9 ± 5.9**	**316.9 ± 69.9**	**397.4 ± 57.1**	**366.6 ± 41.5**	**600.2 ± 83.4**	**644.2 ± 68.3**	**1641 ± 86.4**
P vs $Dd2^{Dd2}$	–	0.002	0.010	0.004	0.010	0.004	0.004	0.052
P vs $Dd2^{Dd2+F145I}$	0.010	–	–	0.29	0.49	0.11	0.032	0.016
md-ADQ IC_{50} (nM)	**26.0 ± 4.8**	**11.7 ± 2.6**	**14.5 ± 2.8**	**18.6 ± 5.9**	**16.2 ± 2.9**	**21.8 ± 1.9**	**23.3 ± 0.6**	**24.1 ± 4.1**
N	5	5	5	4	5	5	4	4
P vs $Dd2^{Dd2}$	–	0.032	0.095	0.19	0.095	0.56	>0.99	0.75
P vs $Dd2^{Dd2+F145I}$	0.095	–	–	0.41	0.22	0.22	0.19	0.11
md-ADQ IC_{90} (nM)	**36.7 ± 7.3**	**16.9 ± 3.1**	**25.7 ± 7.2**	**32.9 ± 8.3**	**31.6 ± 6.1**	**38.9 ± 4.4**	**37.1 ± 4.4**	**36.9 ± 7.1**
P vs $Dd2^{Dd2}$	–	0.016	0.087	0.19	0.15	0.69	>0.99	0.73
P vs $Dd2^{Dd2+F145I}$	0.087	–	–	0.37	0.21	0.21	0.21	0.13
QN IC_{50} (nM)	**245.7 ± 56.5**	**427.7 ± 26.1**	**237.1 ± 37.4**	**220.6 ± 14.8**	**257.2 ± 48.9**	**217.7 ± 5.9**	**240.4 ± 20.1**	**257.2 ± 48.9**
N	5	5	5	4	4	6	6	**4**
P vs $Dd2^{Dd2}$	–	0.032	0.84	0.73	0.90	0.54	0.79	>0.99
P vs $Dd2^{Dd2+F145I}$	0.84	–	–	0.90	0.90	0.79	0.79	0.56
QN IC_{90} (nM)	**745.0 ± 113.2**	**923.2 ± 31.7**	**652.5 ± 75.4**	**709.7 ± 55.4**	**623.5 ± 45.7**	**637.0 ± 73.7**	**663.8 ± 34.3**	**n.d.**
P vs $Dd2^{Dd2}$	–	0.41	0.49	0.89	0.86	0.26	0.76	–
P vs $Dd2^{Dd2+F145I}$	0.49	–	–	0.49	0.23	0.76	0.91	–
PND IC_{50} (nM)	**5.8 ± 0.8**	**6.0 ± 1.0**	**6.0 ± 0.6**	**6.7 ± 1.1**	**6.4 ± 0.9**	**7.9 ± 0.9**	**7.2 ± 0.9**	**3.2 ± 0.6**
N	4	4	4	4	4	6	6	4
P vs $Dd2^{Dd2}$	–	0.89	0.69	0.69	0.69	0.11	0.48	0.11
P vs $Dd2^{Dd2+F145I}$	0.69	–	–	0.49	>0.99	0.25	0.54	0.029
PND IC_{90} (nM)	**9.4 ± 1.3**	**9.6 ± 1.3**	**11.4 ± 0.4**	**12.3 ± 0.9**	**12.3 ± 2.2**	**14.4 ± 2.4**	**9.4 ± 1.4**	**6.4 ± 1.6**
P vs $Dd2^{Dd2}$	–	>0.99	0.11	0.11	0.63	0.20	0.51	0.11
P vs $Dd2^{Dd2+F145I}$	0.11	–	–	0.69	0.49	0.35	0.41	0.057
MFQ IC_{50} (nM)	**7.1 ± 1.0**	**12.2 ± 1.1**	**6.0 ± 1.0**	**5.9 ± 1.0**	**6.4 ± 1.2**	**6.9 ± 0.2**	**5.8 ± 1.1**	**6.0 ± 0.72**
N	6	6	6	5	5	3	4	4
P vs $Dd2^{Dd2}$	–	0.015	0.48	0.54	0.79	0.55	0.61	0.91
P vs $Dd2^{Dd2+F145I}$	0.48	–	–	0.79	0.79	0.55	0.91	0.35
MFQ IC_{90} (nM)	**21.6 ± 3.2**	**31.7 ± 3.6**	**18.5 ± 1.6**	**20.0 ± 2.5**	**19.5 ± 2.5**	**19.8 ± 1.7**	**16.0 ± 1.5**	**14.9 ± 2.3**
P vs $Dd2^{Dd2}$	–	0.18	0.31	0.79	0.54	0.48	0.35	0.26
P vs $Dd2^{Dd2+F145I}$	0.31	–	–	0.33	0.54	0.48	0.39	0.17

IC_{50} and IC_{90} values (nM) are presented as the means ± SEM, as determined in 2 to 7 independent assays perfomed in duplicate. PPQ, piperaquine; CQ, chloroquine; md-CQ, monodesethyl-chloroquine; md-ADQ, monodesethyl-amodiaquine; QN, quinine; PND, pyronaridine; MFQ, mefloquine; N, number of assays. n.d., not determined. Statistical significance was determined via Mann Whitney *U* tests. *P* values are reported for comparisons with the parasite line $Dd2^{Dd2}$ and $Dd2^{Dd2+F145I}$.

$^{*}P < 0.05$	$^{**}P < 0.01$	$^{***}P < 0.001$

Table S3 Transport in proteoliposomes.

Isoform	PPQ			CQ		
	1-min uptake (pmol/mg)	n	*P* v. Dd2+F145I	1-min uptake (pmol/mg)	n	*P* v. Dd2+F145I
Dd2	2.3 ± 0.3	5	0.016	6.5 ± 0.3	6	0.0095
Dd2+F145I	13.6 ± 2.2	4	—	1.9 ± 0.2	4	—
Dd2+F145I+F131C	13.1 ± 2.5	4	>0.99	2.3 ± 0.4	5	0.41
Dd2+F145I+I347T	13.1 ± 2.6	4	>0.99	2.5 ± 0.3	4	0.20
Dd2+F145I+C258W	6.3 ± 0.4	3	0.06	3.9 ± 0.5	3	0.06
3D7	0.5 ± 0.5	5	—	1.2 ± 0.3	4	—

Transport kinetics for ^{3}H-PPQ and ^{3}H-CQ were determined with the listed PfCRT variants reconstituted into proteoliposomes. Data (mean ± SD of n = 3-6 experiments) for the 1-min uptake of ^{3}H-PPQ or ^{3}H-CQ (depicted in **Fig. 2D and 2E**) are shown for each variant tested.

*P <0.05 **P <0.01

Table S4 All salt bridges found for all PfCRT isoforms.

Amino acid pair	Dd2	Dd2+F145I	Dd2+F145I+F131C	Dd2+F145I+I347T	Dd2+F145I+C258W
ASP57/LYS53	43.58	74.33	60.09	68.34	77.96
GLU54/LYS53	15.88	0.73	0.9	5.79	1.3
GLU54/ARG392	21.6	61.45	29.66	23.2	43.21
GLU54/ARG400	5.96	20.04	7.82	0	1.36
ASP57/LYS56	22.9	3.79	7.16	13.45	2.2
ASP57/ARG400	15.45	0	0.03	3.36	0
GLU207/LYS80	3.06	3.6	12.45	1.5	0
ASP368/ARG81	0	0.3	7.26	5.36	14.95
ASP311/LYS85	45.04	36.15	32.99	64.68	61.09
ASP368/LYS85	5.99	7.52	21.54	3.79	15.41
ASP241/LYS116	17.21	1.2	6.62	0.57	3.7
ASP137/ARG231	66.31	0	0	0	0
GLU208/ARG150	18.64	7.22	26.83	16.74	6.49
GLU198/ARG374	0	0	0	0.9	14.51
GLU204/LYS200	67.64	61.95	36.22	48.17	60.85
GLU204/ARG374	0	20.57	2	0.9	0
GLU208/LYS270	13.52	21.74	19.11	13.68	37.62
GLU232/LYS236	53.73	0	0	0	0
GLU271/LYS270	6.36	11.55	7.39	10.72	10.05
GLU271/LYS307	8.06	4.63	13.52	0.7	0
GLU299/LYS307	14.48	9.39	1.66	15.31	10.59
ASP310/LYS307	13.91	1.76	5.19	0.03	2.43
ASP313/LYS317	25	54.96	0.03	0.4	0
ASP338/LYS339	36.05	0	0	0	0
ASP377/ARG374	55.19	34.25	41.51	69.11	22.34
GLU399/ARG392	60.49	64.08	41.81	57.92	36.09
GLU399/LYS402	1.9	3.53	17.64	2.73	15.01

Interaction lifetimes are given as a percentage of time where the interacting species are within 4 Å of each other. Values shown are for interactions that exist for ≥10% of simulation time for at least one isoform. Green indicates a higher percentage and red indicates a low percentage.

Table S5 (page 1) Averaged log_2 fold change of the baseline peptide levels in the variant PfCRT lines versus $Dd2^{Dd2+F145I}$.

Peptide	Mass Spec Mode	Hb chain	$Dd2^{Dd2}$ / $Dd2^{Dd2+F145I}$	$Dd2^{Dd2+F145I+F131C}$ / $Dd2^{Dd2+F145I}$	$Dd2^{Dd2+F145I+I347T}$ / $Dd2^{Dd2+F145I}$	$Dd2^{Dd2+F145I+C258W}$ / $Dd2^{Dd2+F145I}$
AHVD	AHVD_pos	Hbα	1.04	0.36	0.47	
AV;LG;GL;VA	AV;LG;GL;VA_pos	Hbβ	-5.42	0.44	2.29	-3.46
AVMGN	AVMGN_neg	Hbβ	-0.29	-0.05	-0.25	
DALT	DALT_pos	Hbα	-2.48	-0.72	-0.65	
DAVM	DAVM_pos	Hbβ				-3.46
DEVGG	DEVGG_pos	Hbβ	-10.92	0.78	1.30	-3.39
DGLAH	DGLAH_pos;DGLAH_neg	Hbβ				-0.76
DK	DK_pos	Hbα, Hbβ				-0.67
DKFLASV	DKFLASV_pos	Hbα				-4.22
DKL	DKL_neg	Hbβ	-1.51	-0.79	-2.37	-0.52
DLH;HLD	DLH;HLD_neg	Hbα	-11.85	0.50	1.14	
DLHA;AHLD	DLHA;AHLD_pos	Hbβ				-2.77
DLS	DLS_neg	Hbβ	-0.91	-0.37	-1.12	-2.98
DLS;LSD;SDL;SLD	DLS;LSD;SDL;SLD_neg; DLS;LSD;SDL;SLD_pos	Hbα				-0.81
DP	DP_neg	Hbα				-0.54
DPEN	DPEN_neg	Hbβ	0.54	-0.29	-0.95	-2.16
DPENF	DPENF_neg;DPENF_pos	Hbβ				-1.72
DPVN	DPVN_pos	Hbα	0.29	-0.63	-1.37	
DPVNF	DPVNF_neg	Hbα				0.02
ERM	ERM_pos	Hbα				-0.84
ESFGDLSTP	ESFGDLSTP_pos	Hbβ	-8.18	0.21	0.25	-1.39
EV;DL;LD	EV;DL;LD_pos	Hbβ				-1.90
EVG;GDL;STP;DAV;DGL	EVG;GDL;STP;DAV;DGL_pos	Hbβ				-1.14
EVGGEA	EVGGEA_pos	Hbβ				-3.59
FD	FD_pos	Hbα				-1.39
FLSF	FLSF_neg	Hbα	-0.24	-0.33	-0.49	
GA;AG	GA;AG_neg	Hbα, Hbβ				0.21
GAHAGEYGA	GAHAGEYGA_pos	Hbα				0.20
GEALGRLL	GEALGRLL_pos	Hbβ	-1.78	1.07	0.72	
GEYG;SFGD;FSDG	GEYG;SFGD;FSDG_pos	Hbα	-12.02	0.93	0.53	-0.59
GKVGAH;QVKGH	GKVGAH;QVKGH_pos;GKVGAH;QVKGH_neg	Hbα				-0.66
GLAH	GLAH_pos	Hbβ	-0.07	-0.07	-0.08	
GNPK	GNPK_neg	Hbβ	-0.11	-0.65	-0.71	
HFDLSHGSAQ;HVDDMPNALS	HFDLSHGSAQ;HVDDMPNALS_neg	Hbα	-4.40	0.94	1.62	-1.42
HG;GH; HG	HG;GH; HG_pos	Hbα, Hbβ	0.22	-0.54	-0.60	
HGKKV	HGKKV_neg	Hbα, Hbβ				-0.89
HKLRV	HKLRV_pos	Hbα				-1.91
HL;LH	HL;LH_pos	Hbβ				0.02
HLD	HLD_neg	Hbβ				-2.77
HLDNLKG	HLDNLKG_pos	Hbβ	-10.94	0.80	0.75	-2.59
HVDD	HVDD_pos	Hbα	-4.29	0.28	0.22	
KAHGKK	KAHGKK_pos	Hbβ				0.18
KEFT	KEFT_pos	Hbβ				-2.02
KFLASVST	KFLASVST_pos	Hbα	0.29	0.02	0.04	0.37
KGHGK;GHGKK	KGHGK;GHGKK_neg	Hbβ	0.96	0.41	0.43	
KKVADALT;TNVKAAWG;RVDPVNF	KKVADALT;TNVKAAWG;RVDPVNF_pos	Hbα	-2.09	0.80	0.65	
KLRVDPV	KLRVDPV_pos	Hbα				-0.09
KVNVDEV	KVNVDEV_pos	Hbβ				-3.34
LDK	LDK_neg	Hbα				-0.52
LE	LE_pos	Hbα				-0.19
LGR;GRL	LGR;GRL_neg	Hbβ				0.16
LH;HL	LH;HL_pos	Hbα	-9.78	0.83	0.49	
LK;KL	LK;KL_pos	Hbβ	-0.17	0.58	0.12	
LLGNVLVCVLAH	LLGNVLVCVLAH_neg	Hbβ				-2.78
LRVD	LRVD_neg	Hbα	-5.01	1.11	2.28	
LRVDPVN	LRVDPVN_pos	Hbα	0.05	-1.34	-1.24	-0.23
LS;VT;SL;TV	LS;VT;SL;TV_pos	Hbα				-0.09
LSHCLLV	LSHCLLV_pos	Hbα				-2.84
LSPAD	LSPAD_neg	Hbα	-0.19	-0.21	-0.11	
LSPADKTNVKAA	LSPADKTNVKAA_neg	Hbα				-3.59
NP	NP_neg	Hbβ				-4.42
NPKV	NPKV_pos	Hbβ	-10.87	0.29	0.40	
NPKVKAHGKK	NPKVKAHGKK_pos	Hbβ				-4.09
NVDE;DEVGG	NVDE;DEVGG_pos	Hbβ	-11.27	0.78	0.55	
NVDEVG	NVDEVG_pos	Hbβ	-0.07	-0.26	-0.24	
NVDEVGGEALG	NVDEVGGEALG_neg	Hbβ	0.00	-0.66	-0.35	0.19
NVKAA;AQVKG;LRVD	NVKAA;AQVKG;LRVD_neg	Hbα	-7.49	0.81	1.63	-0.23
PA	PA_pos	Hbα	-7.18	0.77	1.98	
PAD;PDA	PAD;PDA_pos	Hbα	-3.69	-1.51	-1.93	-0.09
PAE	PAE_pos	Hbα	-12.24	0.42	0.94	-3.42
PD;DP	PD;DP_pos; PD;DP_neg	Hbβ				-0.54
PDA	PDA_pos	Hbβ	-0.11	0.51	-0.04	0.02
PE	PE_neg	Hbβ	-1.09	-0.62	-0.79	-2.07
PEE	PEE_neg	Hbβ				-0.80
PEEK	PEEK_pos	Hbβ				-1.97
PEN	PEN_pos	Hbβ				-3.26
PENF	PENF_pos	Hbβ	-6.98	0.93	1.87	

Table S5 (page 2) Averaged log_2 fold change of the baseline peptide levels in the variant PfCRT lines versus $Dd2^{Dd2+F145I}$.

Peptide	Mass Spec Mode	Hb chain	$Dd2^{Dd2}$ / $Dd2^{Dd2+F145I}$	$Dd2^{Dd2+F145I+F131C}$ / $Dd2^{Dd2+F145I}$	$Dd2^{Dd2+F145I+I347T}$ / $Dd2^{Dd2+F145I}$	$Dd2^{Dd2+F145I+C258W}$ / $Dd2^{Dd2+F145I}$
PK	PK_pos	Hbβ	-4.73	0.83	1.70	-1.88
PKVK	PKVK_pos	Hbβ				-3.52
PN	PN_neg	Hbα	-10.24	0.53	1.48	
PN;NP	PN;NP_pos	Hbα, Hbβ	-0.98	-0.62	-0.61	
PNA	PNA_pos	Hbα				-4.42
PNALS	PNALS_pos	Hbα				-2.23
PPVQ	PPVQ_neg	Hbβ	-7.96	0.84	1.70	-1.43
PT;TP	PT;TP_pos	Hbα	-8.58	1.00	2.32	-2.88
PTT;DAL	PTT;DAL_pos; PTT;DAL_neg	Hbα, Hbβ				-3.71
PV	PV_pos	Hbα	-10.52	0.97	1.76	-2.38
PVN	PVN_pos	Hbα	-3.03	-1.21	-2.54	-4.52
PVNF	PVNF_neg	Hbβ	-7.46	1.34	2.28	-5.44
PVQ	PVQ_pos	Hbβ				-4.11
PVQA	PVQA_pos	Hbβ	-1.13	-0.43	-0.64	-3.96
PWT	PWT_pos	Hbβ	0.91	-1.63	-2.14	-2.88
PWTQ	PWTQ_pos	Hbβ				-2.84
QKVVA	QKVVA_pos	Hbβ	0.15	0.58	-1.27	
RF;FR	RF;FR_pos	Hbβ	-2.75	1.30	0.64	
SDLHA;HASLD	SDLHA;HASLD_pos	Hbα				-3.66
SFGD;FSDG	SFGD;FSDG_pos	Hbβ	1.97	0.35	0.35	
SFGDLSTP	SFGDLSTP_pos	Hbβ				-0.61
SFPTT	SFPTT_pos	Hbα	-0.19	-0.50	0.07	-3.59
STPDAVM;VDPENF	STPDAVM;VDPENF_neg	Hbβ				-1.48
TLAA	TLAA_neg	Hbα				-0.52
TNVK	TNVK_pos	Hbα				-0.19
TP	TP_neg	Hbβ				-3.44
TPAVH	TPAVH_pos	Hbα	-2.42	1.93	1.02	
TPAVH;KEFT	TPAVH;KEFT_pos	Hbα	0.08	-0.21	-0.30	
TPDA	TPDA_neg	Hbβ				-3.30
TPEE	TPE_pos	Hbα				-3.26
TPEEK;LSTPDA	TPEEK;LSTPDA_pos	Hbβ				-2.20
TSKY	TSKY_neg	Hbα	0.48	0.30	-0.53	
TYFP	TYFP_pos	Hbα	-1.91	-0.52	-0.76	
V	V_pos	Hbα, Hbβ	1.06	-0.06	-0.23	
VAGVANA	VAGVANA_neg	Hbβ	0.64	0.46	0.58	
VAGVANAL	VAGVANAL_neg	Hbβ	0.47	0.36	0.60	
VAHV	VAHV_pos	Hbα	-9.43	-0.16	0.05	
VAHVDDMP	VAHVDDMP_pos	Hbα	-0.39	0.37	0.11	
VC;CV	VC;CV_neg	Hbβ	-9.00	0.70	0.64	-0.42
VD	VD_pos; VD_neg	Hbα, Hbβ	-0.17	0.12	-0.27	-1.98
VDD	VDD_neg; VDD_pos	Hbα	-3.43	0.01	1.21	
VDE;DEV	VDE;DEV_pos	Hbβ	-2.24	2.00	1.67	-1.03
VDEVG	VDEVG_pos	Hbβ				-2.18
VDEVGGEALG	VDEVGGEALG_neg	Hbβ	0.72	0.40	0.44	
VDPENF	VDPENF_pos	Hbβ	-0.80	-0.91	-1.61	
VDPVN	VDPVN_neg	Hbα				-2.44
VG	VG_neg	Hbα	-0.18	0.33	0.11	-3.62
VG;GV	VG;GV_neg;VG;GV_pos	Hbβ				-3.39
VHAS	VHAS_pos	Hbα	-0.81	-0.68	-1.17	
VHASL	VHASL_neg	Hbα				-3.39
VHL;LHV	VHL;LHV_pos	Hbβ				0.30
VLSP	VLSP_pos	Hbα	-1.44	-0.89	-1.87	
VNVDEVG;EVGGEALG	VNVDEVG;EVGGEALG_neg	Hbβ				0.17
VT;LS	VT;LS_pos	Hbβ	-2.16	0.69	-0.29	
VV	VV_pos	Hbβ	-0.04	0.15	-0.07	
VVYP	VVYP_neg	Hbβ				-0.79
YH	YH_pos	Hbβ				-0.61

134 peptides were detected in either positive or negative mode. Blank spaces denote missing or undetectable values.

Table S6 (page 1) List of peptides showing significantly different levels for $Dd2^{Dd2}$, $Dd2^{Dd2+F145I+F131C}$, $Dd2^{Dd2+F145I+I347T}$, and $Dd2^{Dd2+F145I+C258W}$ compared to $Dd2^{Dd2+F145I}$.

Peptide	IEP	pH at 5.5	pH at 7.4	*P*-value	Mean of log2-transformed peak areas of $Dd2^{Dd2+F145I}$	Mean of log2-transformed peak areas of $Dd2^{Dd2}$	Difference in log_2-transformed mean peak areas	SE of difference
AHVD	4.78	-0.4	-1	0.048	14.3	15.3	1.0	0.36
AV;LG;GL;VA	5.98; 5.98; 5.98; 5.98	0; 0; 0; 0	0; 0; 0; 0	0.009	11.0	5.6	-5.4	1.05
DGLAH	4.78	-0.4	-1	0.001	12.2	1.3	-10.9	0.68
DLHA;AHLD	4.78; 4.78	-0.4; 0.4	-1; -1	0.002	14.9	3.1	-11.9	0.80
EV;DL;LD	3.64; 3.37; 3.37	-0.9; -1; -1	-1;-1; -1	0.0002	14.7	6.5	-8.2	0.63
GKVGAH;QVKGH	9.37	3.2	2	0.0001	17.1	5.1	-12.0	0.57
HG;GH	7.61	1.7	0	0.003	12.3	7.9	-4.4	0.30
HVDD	3.93	-1.4	-2	0.00002	15.0	4.1	-10.9	0.40
KKVADALT;TNVKAAWG;RVDPVNF	8.76; 9.07; 6.5	1; 1; 0	0.9; 1; 0	0.011	15.0	15.9	15.0	0.96
LH;HL	7.37; 7.37	1.2; 1.2	0; 0	0.00003	12.8	3.1	-9.8	0.47
LRVDPVN	6.5	0	0	0.011	10.6	5.6	-5.0	0.85
NPKVKAHGKK	9.66	4.6	3.9	0.001	11.8	0.9	-10.9	0.78
NVDE;DEVGG	3.29; 3.29	-1.9; -1.9	-2; -2	0.017	14.2	10.4	-3.8	0.86
NVDEVG	3.29	-1.9	-2	0.0001	16.1	4.8	-11.3	0.36
PA	5.98	0	0	0.001	11.7	4.2	-7.5	0.49
PAD;PDA	3.17; 3.17	-2; -2	-2; -2	0.005	10.1	3.0	-7.2	0.93
PD;DP	3.37; 3.37	-2; -2	-2; -2	0.00001	15.1	2.9	-0.1	0.40
PK	9.07	1	1	0.001	12.5	5.5	-7.0	0.76
PKVK	9.37	2	1.9	0.004	11.3	6.6	-4.7	0.76
PN;NP	5.98; 5.98	0; 0	0; 0	0.0004	12.1	1.9	-10.2	0.63
PT;TP	5.98; 5.98	0; 0	0; 0	0.0001	12.9	4.9	-8.0	0.54
PTT;DAL	5.98; 3.37	0; -1	0; -1	0.008	12.2	3.6	-8.6	0.94
PVN	5.98	0	0	0.0001	13.5	3.0	-10.5	0.64
PVNF	5.98	0	0	0.005	14.7	11.7	-3.0	0.54
PVQ	5.98	0	0	0.001	11.0	3.5	-7.5	0.70
VAHVDDMP	3.93	-1.4	-2	0.002	14.0	4.6	-9.4	0.89
VD	3.37	-1	-1	0.005	11.6	2.6	-9.0	0.77

Peptide	IEP	pH at 5.5	pH at 7.4	*P*-value	Mean of log2-transformed peak areas of $Dd2^{Dd2+F145I}$	Mean of log2-transformed peak areas of $Dd2^{Dd2+F145I+F131C}$	Difference in log_2-transformed mean peak areas	SE of difference
NVDE;DEVGG	3.29	-1.9	-2	0.037	14.2	16.0	1.8	0.57

Peptide	IEP	pH at 5.5	pH at 7.4	*P*-value	Mean of log2-transformed peak areas of $Dd2^{Dd2+F145I}$	Mean of log2-transformed peak areas of $Dd2^{Dd2+F145I+I347T}$	Difference in log_2-transformed mean peak areas	SE of difference
DGLAH	4.78	-0.4	-1	0.025	12.2	13.5	1.3	0.34
DLHA;AHLD	4.78; 4.78	-0.4; 0.4	-1; -1	0.029	14.9	16.1	1.1	0.29
HG;GH	7.37; 7.37	0.6; 0.6	0; 0	0.023	12.3	13.9	1.6	0.45
PA	5.98	0	0	0.048	11.7	13.3	1.6	0.47
PAD;PDA	3.17	-2	-2	0.043	10.1	12.1	2.0	0.67
PN;NP	5.98	0	0	0.026	12.1	13.6	1.5	0.35
PT;TP	5.98	0	0	0.022	12.9	14.6	1.7	0.45
PVN	5.98	0	0	0.040	13.5	15.3	1.8	0.55

Table S6 (page 2) List of peptides showing significantly different levels for $Dd2^{Dd2}$, $Dd2^{Dd2+F145I+F131C}$, $Dd2^{Dd2+F145I+I347T}$, and $Dd2^{Dd2+F145I+C258W}$ compared to $Dd2^{Dd2+F145I}$.

Peptide	IEP	pH at 5.5	pH at 7.4	*P*-value	Mean of log2-transformed peak areas of $Dd2^{Dd2+F145I}$	Mean of log2-transformed peak areas of $Dd2^{Dd2+F145I+C258W}$	Difference in log_2-transformed mean peak areas	SE of difference
AV;LG;GL;VA	5.98; 5.98; 5.98; 5.98	0; 0; 0; 0	0; 0; 0; 0	0.002	13.6	10.2	-3.5	0.51
DEVGG	3.29	-1.9	-2	0.008	14.5	11.1	-3.4	0.61
DKFLASV	6.34	0	0	0.001	15.5	11.3	-4.2	0.35
DLH	4.77	-0.8	-2	0.025	15.8	13.1	-2.8	0.70
DMPNA	3.37	-1	-1	0.031	13.5	12.1	-1.4	0.42
EVGGEA	3.02	-1.8	-2	0.040	12.5	8.9	-3.6	1.00
HLD	4.78	-0.4	-1	0.025	15.8	13.1	-2.8	0.70
KVNVDEV	4.19	-0.9	-1	0.046	13.7	10.4	-3.3	1.13
LSHCLLV	6.59	0.6	-0.4	0.026	13.9	11.1	-2.8	0.72
LSPAD	3.37	-1	-1	0.013	13.6	10.0	-3.6	0.74
NP	5.98	0	0	0.004	15.3	10.9	-4.4	0.69
NPKV	9.07	1	1	0.028	17.4	13.3	-4.1	0.88
PAE	3.64	-0.9	-1	0.021	14.2	10.8	-3.4	0.81
PEEK	4.44	-0.8	-1	0.034	17.6	15.7	-2.0	0.51
PEN	3.64	-0.9	-1	0.020	15.2	12.0	-3.3	0.77
PENF	3.64	-0.9	-1	0.027	14.7	12.8	-1.9	0.44
PN	5.98	0	0	0.004	15.3	10.9	-4.4	0.69
PTT;DAL	5.98; 3.37	0; -1	0; -1	0.019	12.7	9.0	-3.7	0.85
PVN	5.98	0	0	0.044	16.9	12.4	-4.5	1.18
PVNF	5.98	0	0	0.001	15.4	10.0	-5.4	0.69
PVQ	5.98	0	0	0.012	13.6	9.5	-4.1	0.92
PVQA	5.98	0	0	0.009	15.7	11.8	-4.0	0.77
PWTQ	5.98	0	0	0.026	13.9	11.1	-2.8	0.72
QKVVA	9.07	1	1	0.005	13.3	9.6	-3.7	0.66
TP	5.98	0	0	0.039	14.8	11.3	-3.4	0.92
TPAVH	7.37	0.6	0	0.036	18.1	14.8	-3.3	0.81
TPDAV	3.37	-1	-1	0.013	13.6	10.0	-3.6	0.74
TPE	3.64	-0.9	-1	0.020	15.2	12.0	-3.3	0.77
VG	5.98	0	0	0.002	13.2	9.5	-3.6	0.44
VG;GV	5.98; 5.98	0; 0	0; 0	0.012	14.5	11.1	-3.4	0.46
VHAS	7.37	0.6	0	0.012	14.5	11.1	-3.4	0.46

Data were obtained from three independent experiments with technical triplicates. For each peptide, the isoelectric point (IEP), pH at 5.5, and pH 7.4 are displayed. *P* values were calculated from unpaired *t* tests. Gray indicates peptides that were detected in more than one line.

Table S7 List of oligonucleotides used in this study.

Name	Nucleotide Sequence (5'-3')	Description	Lab name	Purpose
p1	CCCTTGTCGACCTTAACAGATGGCTC	*pfcrt* exon 2 SalI Fwd	p3519	Sequencing primer for *pfcrt*.
p2	TCAAACATGACAAGGGAAATAGT	*pfcrt* exon 5 Rev	p2427	
p3	CTCGAGatggttggttcgctaaactgc	hDHFR XhoI Fwd	p3315	Integration PCR #1. 2.5 kb yes/no. integration at 3' end Sequences exons 2-3.
p4	TTGACCCTTATATATTCCACCCA	*pfcrt* 3' UTR	p3403	
p5	cttgggCCCAAGTTGTACTGCTTCTAAGC	*pfcrt* 5' UTR (-494-517) ApaI Fwd	p3404	Integration PCR #2. 1.2 kb checks integration at 5' end (1.4 kb if unedited due to additional intron 2).
p6	cttatcgatAAGCAGAAGAACATATTAATAG GAATACTTAATTG	*pfcrt* exon 3 ClaI Rev	p3265	
p7	GACCTTAACAGATGGCTCAC	*pfcrt* exon 2 EcoRI Fwd	p3264	Integration PCR #3 primer (along with p6). 0.4 kb (0.6 kb if unedited due to additional intron 2). Sequences exons 2-3.
p8	aaccatggatTTATTGTGTAATAATTGAATCGACG	pfcrt exon 13 Rev	p1640	Integration PCR #4 primer (along with p5). 2 kb. Sequence entire edited locus.
p9	agccGGTGATGTTGTAAgAGAACCAAGATTATTAG	PfCRT F131C SDM Fwd	p7068	PfCRT F131C SDM
p10	CTAATAATCTTGGTTCTcTTACAACATCACCggct	PfCRT F131C SDM Rev	p7069	
p11	CCTGTTCAGTCATTTTGGCCaTCATAGGTCTTACA AGAACTAC	PfCRT F145I SDM Fwd	p6106	PfCRT F145I SDM
p12	GTAGTTCTTGTAAGACCTATGAtGGCCAAAATGAC TGAACAGG	PfCRT F145I SDM Rev	p6107	
p13	ctttttccaattgttcacttcttgGcttatattac ctgtatacaccctt	PfCRT C258W SDM Fwd	p8550	PfCRT C258W SDM
p14	aagggtgtatacaggtaatataagCcaagaagtga acaattggaaaaag	PfCRT C258W SDM Rev	p8551	
p15	aaattttctaccatgacatatactaCtgttagttg tatacaaggtccagca	PfCRT I347T SDM Fwd	p7374	PfCRT I347T SDM
p16	tgctggaccttgtatacaactaacaGtagtatatg tcatggtagaaaattt	PfCRT I347T SDM Rev	p7375	
p17	GAAGCTTTAATTTACAATTTTgTGCTATATCCATG TTAGATGCC	PfCRT F131C SDM Fwd	p8136	F131C SDM on *pfcrt* sequence codon optimized for S. *cerevisiae.*
p18	GGCATCTAACATGGATATAGCAcAAAATTGTAAAT TAAAGCTTC	PfCRT F131C SDM Rev	p8137	
p19	GCAGCGTCATCTTGGCCaTCATCGGTCTTACCAGA AC	PfCRT F145I SDM Fwd	p7698	F145I SDM on *pfcrt* sequence codon optimized for S. *cerevisiae.*
p20	GTTCTGGTAAGACCGATGAtGGCCAAGATGACGCT GC	PfCRT F145I SDM Rev	p7699	
p21	GTTAGCTTCTTCCAACTGTTCACTTCATGgTTAAT CCTGCCAGTTTACACACTACCATTC	PfCRT C258W SDM Fwd	p8821	C258W SDM on *pfcrt* sequence codon optimized for S. *cerevisiae.*
p22	GAATGGTAGTGTGTAAACTGGCAGGATTAAcCATG AAGTGAACAGTTGGAAGAAGCTAAC	PfCRT C258W SDM Rev	p8822	
p23	CTCCACCATGACTTACACTAcTGTGAGTTGCATCC AGGGGC	PfCRT I347T SDM Fwd	p8138	I347T SDM on *pfcrt* sequence codon optimized for S. *cerevisiae.*
p24	GCCCCTGGATGCAACTCACAgTAGTGTAAGTCATG GTGGAG	PfCRT I347T SDM Rev	p8139	
p25	CCGCGACTAGTGAGCTCGTCGAC	pFastBac Sequencing	p8157	pFastBac constructs sequencing primer

Fwd, forward primer; Rev, reverse; SDM, site-directed mutagenesis; UTR, untranslated region.

SUPPLEMENTARY REFERENCES

1. Straimer J, Lee MC, Lee AH, Zeitler B, Williams AE, Pearl JR, Zhang L, Rebar EJ, Gregory PD, Llinas M, Urnov FD, Fidock DA. 2012. Site-specific genome editing in *Plasmodium falciparum* using engineered zinc-finger nucleases. Nat Methods 9:993-8.
2. Kim J, Tan YZ, Wicht KJ, Erramilli SK, Dhingra SK, Okombo J, Vendome J, Hagenah LM, Giacometti SI, Warren AL, Nosol K, Roepe PD, Potter CS, Carragher B, Kossiakoff AA, Quick M, Fidock DA, Mancia F. 2019. Structure and drug resistance of the *Plasmodium falciparum* transporter PfCRT. Nature 576:315-320.
3. Willems A, Kalaw A, Ecer A, Kotwal A, Roepe LD, Roepe PD. 2023. Structures of *Plasmodium falciparum* Chloroquine Resistance Transporter (PfCRT) isoforms and their interactions with chloroquine. Biochemistry 62:1093-1110.